

RESEARCH ARTICLE

The dinucleotide composition of the Zika virus genome is shaped by conflicting evolutionary pressures in mammalian hosts and mosquito vectors

Jelke J. Fros^{1,2*}, Imke Visser^{2,3}, Bing Tang³, Kexin Yan³, Eri Nakayama^{3,4}, Tessa M. Visser⁵, Constantianus J. M. Koenraadt⁵, Monique M. van Oers², Gorbien P. Pijlman², Andreas Suhrbier³, Peter Simmonds¹

1 Nuffield Department of Medicine, Peter Medawar Building for Pathogen Research, University of Oxford, Oxford, United Kingdom, **2** Laboratory of Virology, Wageningen University and Research, Wageningen, the Netherlands, **3** QIMR Berghofer Medical Research Institute, Brisbane, Queensland, Australia, **4** Department of Virology I, National Institute of Infectious Diseases, Tokyo, Japan, **5** Laboratory of Entomology, Wageningen University and Research, Wageningen, the Netherlands

* jelke.fros@wur.nl



OPEN ACCESS

Citation: Fros JJ, Visser I, Tang B, Yan K, Nakayama E, Visser TM, et al. (2021) The dinucleotide composition of the Zika virus genome is shaped by conflicting evolutionary pressures in mammalian hosts and mosquito vectors. *PLoS Biol* 19(4): e3001201. <https://doi.org/10.1371/journal.pbio.3001201>

Academic Editor: Claudia Bank, University of Bern, SWITZERLAND

Received: July 24, 2020

Accepted: March 23, 2021

Published: April 19, 2021

Copyright: © 2021 Fros et al. This is an open access article distributed under the terms of the [Creative Commons Attribution License](https://creativecommons.org/licenses/by/4.0/), which permits unrestricted use, distribution, and reproduction in any medium, provided the original author and source are credited.

Data Availability Statement: All relevant data are within the paper and its [Supporting Information](#) files.

Funding: J.F. was supported by the Wageningen Graduate School Postdoc Talent Programme WGS-2016-23 (www.pe-rc.nl/node/20897). P.S. is supported by Wellcome investigator award WT103767MA (<https://wellcome.ac.uk/>). A. S. is a leadership fellow of the National Health and Medical Research Council (www.nhmrc.gov.au/) of

Abstract

Most vertebrate RNA viruses show pervasive suppression of CpG and UpA dinucleotides, closely resembling the dinucleotide composition of host cell transcriptomes. In contrast, CpG suppression is absent in both invertebrate mRNA and RNA viruses that exclusively infect arthropods. Arthropod-borne (arbo) viruses are transmitted between vertebrate hosts by invertebrate vectors and thus encounter potentially conflicting evolutionary pressures in the different cytoplasmic environments. Using a newly developed Zika virus (ZIKV) model, we have investigated how demands for CpG suppression in vertebrate cells can be reconciled with potentially quite different compositional requirements in invertebrates and how this affects ZIKV replication and transmission. Mutant viruses with synonymously elevated CpG or UpA dinucleotide frequencies showed attenuated replication in vertebrate cell lines, which was rescued by knockout of the zinc-finger antiviral protein (ZAP). Conversely, in mosquito cells, ZIKV mutants with elevated CpG dinucleotide frequencies showed substantially enhanced replication compared to wild type. Host-driven effects on virus replication attenuation and enhancement were even more apparent in mouse and mosquito models. Infections with CpG- or UpA-high ZIKV mutants in mice did not cause typical ZIKV-induced tissue damage and completely protected mice during subsequent challenge with wild-type virus, which demonstrates their potential as live-attenuated vaccines. In contrast, the CpG-high mutants displayed enhanced replication in *Aedes aegypti* mosquitoes and a larger proportion of mosquitoes carried infectious virus in their saliva. These findings show that mosquito cells are also capable of discriminating RNA based on dinucleotide composition. However, the evolutionary pressure on the CpG dinucleotides of viral genomes in arthropod vectors directly opposes the pressure present in vertebrate host cells, which provides evidence that an adaptive compromise is required for arbovirus transmission. This suggests

Australia (APP1173880) which in part funded this research via project grant APP1144950. The funders had no role in study design, data collection and analysis, decision to publish, or preparation of the manuscript.

Competing interests: The authors have declared that no competing interests exist.

Abbreviations: ANOVA, analysis of variance; arbo, arthropod-borne; CAI, codon adaptation index; CPE, cytopathic effect; DMEM, Dulbecco's modified Eagle medium; dpi, days postinfection; E7, echovirus 7; eIF4A, eukaryotic translation initiation factor 4A; EPDA, end-point dilution assay; FBS, fetal bovine serum; FDR, false discovery rate; ISF, insect-specific flavivirus; MBFV, mosquito-borne flavivirus; MFED, minimal free energy difference; NKVF, no known vector flavivirus; OAS1, 2'-5'-oligoadenylate synthetase 1; OAS3, 2'-5'-oligoadenylate synthetase 3; O/E, observed over the expected; ORF, open reading frame; PBS, phosphate buffered saline; qRT-PCR, real-time quantitative reverse transcription PCR; RH, relative humidity; RNAi, RNA interference; RNaseL, ribonuclease L; RPMI, Roswell Park Memorial Institute; s.c., subcutaneously; SCR, scrambled control virus; siRNA, small interfering RNA; SSV, synonymous site variability; TBFV, tick-borne flavivirus; WT, wild-type; ZAP, zinc-finger antiviral protein; ZIKV, Zika virus.

that the genome composition of arbo flaviviruses is crucial to maintain the balance between high-level replication in the vertebrate host and persistent replication in the mosquito vector.

Introduction

Arthropod-borne viruses (arboviruses) are transmitted between vertebrate hosts by invertebrate arthropod vectors such as mosquitoes, ticks, biting midges, and sand flies. When hematophagous vectors feed on infected vertebrate hosts, the virus first needs to enter and pass through the vector's midgut endothelial cells and persistently infect other tissues to disseminate into the vector's salivary glands before the arbovirus is transmitted to the next vertebrate host during subsequent feeding events. Transmission of arboviruses thus requires active virus replication in 2 evolutionary distant hosts that are separated by more than 500 million years of evolution [1]. Hence, arboviruses encounter divergent cellular and molecular environments, exemplified by the different antiviral responses that vertebrate hosts and invertebrate vectors rely on to cope with viral infections. Vertebrate animals possess a plethora of innate and adaptive antiviral immune responses [2], while invertebrates largely rely on RNA interference (RNAi) to control viral infections [3,4]. As intracellular pathogens, all viruses rely on cellular machinery for their replication, which exposes viruses to the intracellular milieu of the host cell. The transmission cycle of arboviruses places them in 2 distinct intracellular environments with dissimilar adaptive pressures for replication and evasion of host antiviral responses (reviewed in [5]). How arboviruses are able to thrive while continuously alternating between these distinct cellular environments remains an intriguing research topic [6].

One of the most striking molecular differences between vertebrate and invertebrate organisms is the dinucleotide usage in their genomic DNA and coding mRNA sequences. In the DNA of vertebrates, the dinucleotide combination of a cytosine followed by a guanine (CpG) occurs less frequently than predicted, based on frequencies of C and G mononucleotides. The cytosine in CpG is prone to methylation, which can cause the cytosine to deaminate and mutate into a thymine [7,8]. In contrast, the genome of most invertebrates contains largely unbiased frequencies of CpG dinucleotides, reflecting greatly reduced DNA methylation activity [9]. Both vertebrates and invertebrates have additionally evolved to reduce UpA dinucleotide frequencies in their mRNA through a range of mechanisms largely related to mRNA stability [10,11]. Most viruses with RNA genomes have evolved to mirror the dinucleotide usage of their host's mRNA, with invertebrate viruses solely suppressing UpA dinucleotides and vertebrate viruses underrepresenting both UpA and CpG dinucleotides, even though CpGs in viral RNA are not subjected to the same methylation and mutation pressure that acts on vertebrate host DNA [12–14].

Artificially increasing CpG or UpA dinucleotide frequencies through hundreds of synonymous mutations effectively attenuates the replication of multiple RNA viruses in vertebrate cell cultures [15–19]. Vertebrate cells identify unnaturally elevated levels of CpG dinucleotides as non-self, mediated by the zinc-finger antiviral protein (ZAP) [16,20–22]. We previously showed that ZAP is also required for the attenuation of UpA-high mutants of echovirus 7 (E7) (genus *Enterovirus B*, family *Picornaviridae*) [21]. ZAP is interconnected with the interferon response and can modulate translation initiation through the sequestration of eukaryotic translation initiation factor 4A (eIF4A) [23–25]. ZAP is additionally associated with cellular RNA degradation, with links to stress granule and processing body components as well as to the endonuclease RNase L activated by 2'-5'-oligoadenylate synthetase 3 (OAS3), the 3'-5' exosomal, and the 5'-3' XRN1-mediated RNA degradation pathways [20,26–28]. Together, this

indicates that vertebrate ZAP is involved in the detection of both UpA and CpG dinucleotides and recruits diverse host cell proteins to inhibit virus replication [21,29,30].

Whether invertebrate cells possess similar non-self RNA detection mechanisms and whether alternating between vertebrate hosts and arthropod vectors puts additional selective pressure on arboviruses is currently unknown. The lack of CpG suppression in invertebrates and their viruses suggests the absence of selection pressure against CpGs in arthropods, while UpA dinucleotides are clearly underrepresented in both arthropods and their viruses [13,14]. We therefore hypothesized that the selection pressures on UpA dinucleotides would be similar in vertebrate hosts and arthropod vectors, while the selection pressure on CpG dinucleotides may be absent in these vectors. To investigate the constraints that an arbovirus encounters during its transmission cycle, we turned to the genus *Flavivirus* (family *Flaviviridae*). This genus contains many clinically relevant arboviruses, which include mosquito-borne flaviviruses (MBFV), e.g., Zika virus (ZIKV), dengue virus, West Nile virus, Japanese encephalitis virus, and yellow fever virus, as well as a number of tick-borne flaviviruses (TBFV), e.g., tick-borne encephalitis virus. In addition to arboviruses, the genus *Flavivirus* also contains members with no known vector (NKVF) and insect-specific flaviviruses (ISF). The latter are unable to infect vertebrates and exclusively replicate in insects and cultured insect cells [31]. To investigate whether arbovirus genome composition is subject to distinct evolutionary pressures in vertebrate host and arthropod vectors, we constructed ZIKV mutants with synonymously increased CpG or UpA dinucleotide frequencies and tested their replication kinetics in vertebrate and invertebrate cells, mice, and mosquitoes.

Results

Flavivirus genome composition and mutant Zika virus design

To compare the CpG and UpA dinucleotide usage between different flaviviruses, the ratio of CpG and UpA dinucleotide frequencies from full-length flavivirus genome sequences were plotted as the observed over the expected (O/E) frequencies (Fig 1A, large data points). Viral sequence data were superimposed onto large randomly selected sets of vertebrate (*Homo sapiens*) and invertebrate mosquito (*Aedes aegypti*) mRNAs (Fig 1A, small data points). Both human host and mosquito vector mRNA suppress UpA dinucleotides (y-axis), while only human mRNA underrepresents CpG dinucleotides (x-axis). All flaviviruses that infect vertebrates (i.e., MBFV, TBFV, and NKVF) have clearly adapted to mimic the genome composition of the vertebrate host, with marked underrepresentation of both CpG and UpA dinucleotides. In contrast, the ISFs and particularly the phylogenetically most distant lineage I ISFs contain a much higher ratio of CpG dinucleotides frequencies, more closely resembling the unbiased CpG frequency found in their arthropod hosts. Lineage II ISFs display an insect-specific phenotype and contain more CpG dinucleotides than vertebrate-infecting flaviviruses, while phylogenetically they cluster together with MBFVs (Fig 1A) [14,31–34].

To investigate the biological role of CpG and UpA suppression in a typical MBFV, ZIKV mutants were created with increased frequencies of either CpG or UpA dinucleotides by introducing many synonymous changes into a 1654 nucleotide long, coding region of the viral genome (Fig 1B). The complete genome of wild-type (WT) ZIKV has ratios of 0.42 and 0.52 for the O/E frequencies of CpG and UpA dinucleotides, respectively. The selected region contains 53 CpG and 57 UpA dinucleotides with comparable CpG and UpA suppression (detailed in S1 Table). Before introducing any mutations, we confirmed that the ZIKV open reading frame (ORF), except for the 5'-end which contains the cyclisation sequence [35], has a relatively uniform nucleotide variability at synonymous sites and low minimal free energy differences (MFED) (Fig 1C). This suggests that, apart from conserving amino acid sequence, there

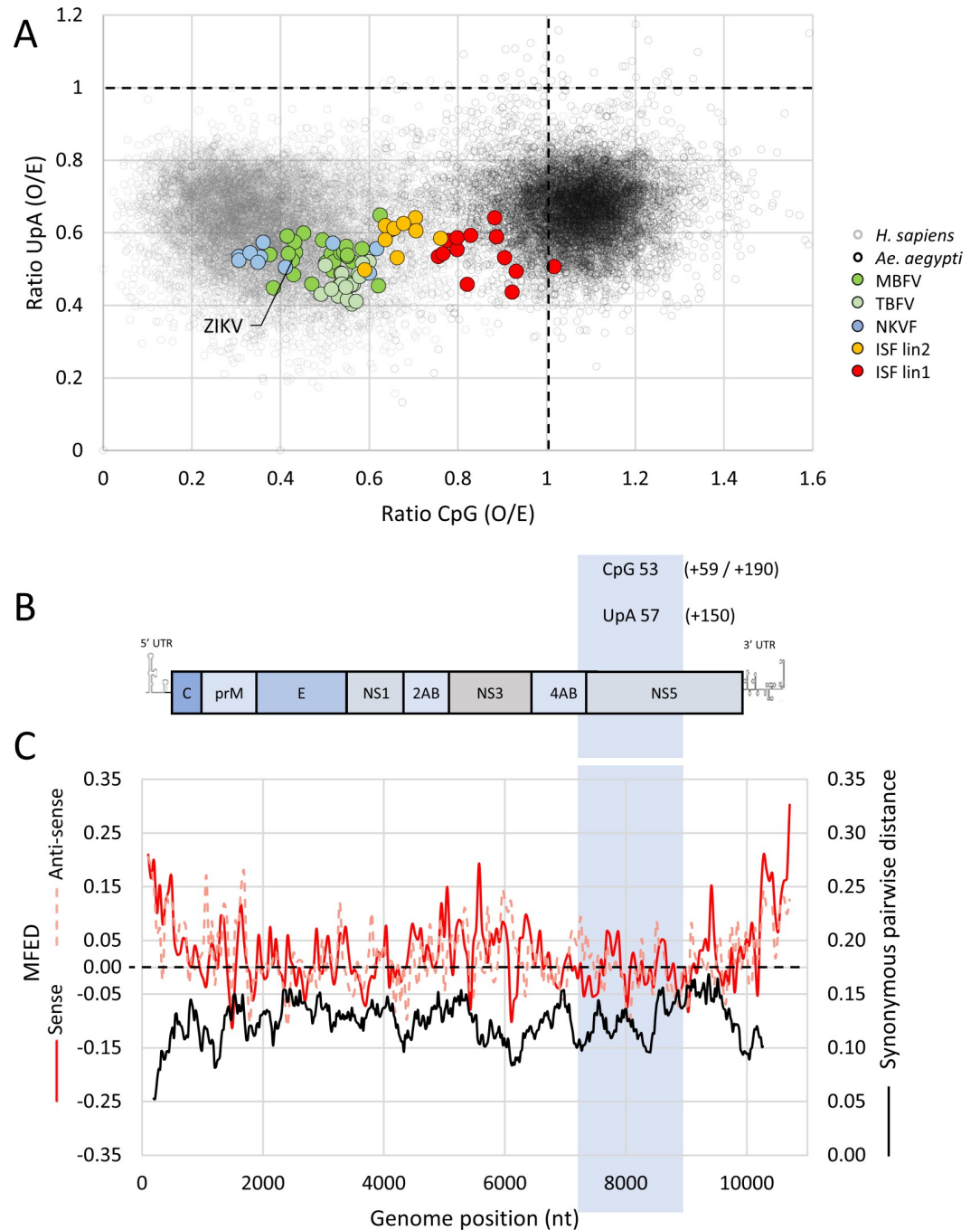


Fig 1. Flavivirus CpG and UpA dinucleotide usage, Zika virus genome organization, and the position of the mutated region. (A) Data points represent the ratio of CpG (x-axis) and UpA (y-axis) dinucleotides in individual RNA sequences. Small data points denote human mRNAs (gray) and mosquito mRNAs (black). Large data points represent full-length genome sequences of flavivirus species with MBFV (green), TBFV (light green), NKVF (blue), and the lineage 1 and 2 ISF (red and orange), respectively. The O/E ratio of 1.0 (dotted lines) is the mathematically expected frequency of occurrence if the RNA's mononucleotides were randomly distributed. (B) Schematic representation of the ZIKV genome, with the mutated region boxed and displaying the number of CpG and UpA dinucleotides in wild-type ZIKV. Additional CpG and UpA dinucleotides of the CpG_1.0 (+59), CpG_max (+190), and UpA_max (+150) mutant viruses are listed in brackets. (C) MFED and synonymous pairwise distance (black line) were calculated for 19 ZIKV isolates that were >1% dissimilar in nucleotide sequences using a fragment size of 200 with 48 nucleotide increments for MFED and sliding window of 21 codons for synonymous pairwise distance that were >1% dissimilar in nucleotide sequences using a fragment size of 200 with 48 nucleotide increments for MFED and sliding window of 21 codons for synonymous pairwise distance as used in

previous analyses of echovirus 7 and murine norovirus [19,59]. MFED values of both the sense (red line) and the antisense (dashed pink line) strand in the selected region are close to the null expectation (dotted black line). Please refer to [S1 Data](#) for the numerical values underlying panels A and C. Values were calculated using SSE software v1.4. ISF, insect-specific flavivirus; MBFV, mosquito-borne flavivirus; MFED, minimal free energy difference; NKVF, no known vector flavivirus; O/E, observed/expected; TBFV, tick-borne flavivirus; ZIKV, Zika virus.

<https://doi.org/10.1371/journal.pbio.3001201.g001>

are no other conserved nucleotide sequences or critical RNA structures in the ZIKV ORF. To confirm the absence of critical RNA sequences experimentally, a scrambled control virus (SCR) was designed that contained extensive synonymous changes in the target region but retained WT dinucleotide frequencies. Furthermore, we created mutants that maximally overrepresented CpG or UpA dinucleotides, without altering the number of the other UpA or CpG dinucleotide or the encoded amino acid sequence. This resulted in the CpG_max ZIKV mutant with 190 additional CpG dinucleotides and an O/E ratio of 1.62 and the UpA_max ZIKV mutant (+ 150 UpA dinucleotides, O/E ratio 1.72). As the genome of *Ae. aegypti*, the main mosquito vector for ZIKV, shows no suppression of CpG dinucleotides (O/E ratio approximately 1.0) (Fig 1A), we additionally created a mutant virus with synonymously increased CpG dinucleotides to the unsuppressed (mosquito-like) ratio of 1.0 (termed CpG_1.0) by addition of 59 CpG dinucleotides. We made use of an infectious cDNA clone to generate virus stocks of these ZIKV mutants in Vero E6 cells. As the fitness between the ZIKV mutants was expected to vary substantially, we used equal numbers of viral RNA copies to infect cells.

ZIKV with elevated CpG or UpA dinucleotide frequencies is attenuated in vertebrate cell cultures

Vertebrate cell lines were infected with the different mutant ZIKV stocks to investigate the replication kinetics of the mutant viruses. Samples were taken daily from cell culture supernatants and checked for the presence of infectious virus (Fig 2). In all cases, the SCR control behaved very similarly to the WT, indicating that the introduced synonymous changes did not affect virus replication. In vertebrate Vero E6 cells and A549 cells, UpA_max ZIKV was clearly attenuated with approximately 10-fold lower titers of progeny virus at any time postinfection. The CpG_max ZIKV mutant displayed 2- to 3-fold lower titers compared to WT, while the replication kinetics of the CpG_1.0 mutant virus were similar to that of the WT virus (Fig 2A and 2B). At 2 days postinfection, CpG_max and UpA_max virus differed significantly from WT and the SCR control (Fig 2D) (two-way ANOVA, $F(4, 30) = 6.315, p < 0.05$). Knockout of ZAP rescued the attenuated phenotype of the CpG_max ZIKV mutant, compared to that in wild-type A549 cells (Fig 2C and 2D) (two-way ANOVA, $F(1, 30) = 11.49, p < 0.05$). Although replication of the UpA_max ZIKV mutant appeared similarly rescued by knockout of ZAP (Fig 2B–2D), this was not significantly different from replication in wild-type A549 cells ($p = 0.06$). Similar to what was reported previously for CpG-high E7 mutants [21], knockout of ribonuclease L (RNaseL) or OAS3 resulted in comparable replication rates between CpG_max and WT ZIKV to WT levels (Fig 2 and S1A–S1C Fig).

The cytopathic effects (CPE) caused by ZIKV infections in A549 cells were mild; however, delays in CPE for the CpG_1.0, CpG_max, and UpA_max viruses were observed. To investigate replication phenotypes further, a plaque assay was performed and plaque sizes were determined by immunostaining as a measure for the rate at which infectious virus spread through the culture. Three days postinoculation with WT ZIKV and SCR ZIKV, large plaques with an average diameter just over 1,000 μm were observed in parental A549 cells (Fig 2E and S1D Fig). Inoculation with CpG_1.0 ZIKV resulted in slightly smaller average plaque diameters (approximately 750 μm), while the CpG_max and UpA_max ZIKV mutants displayed

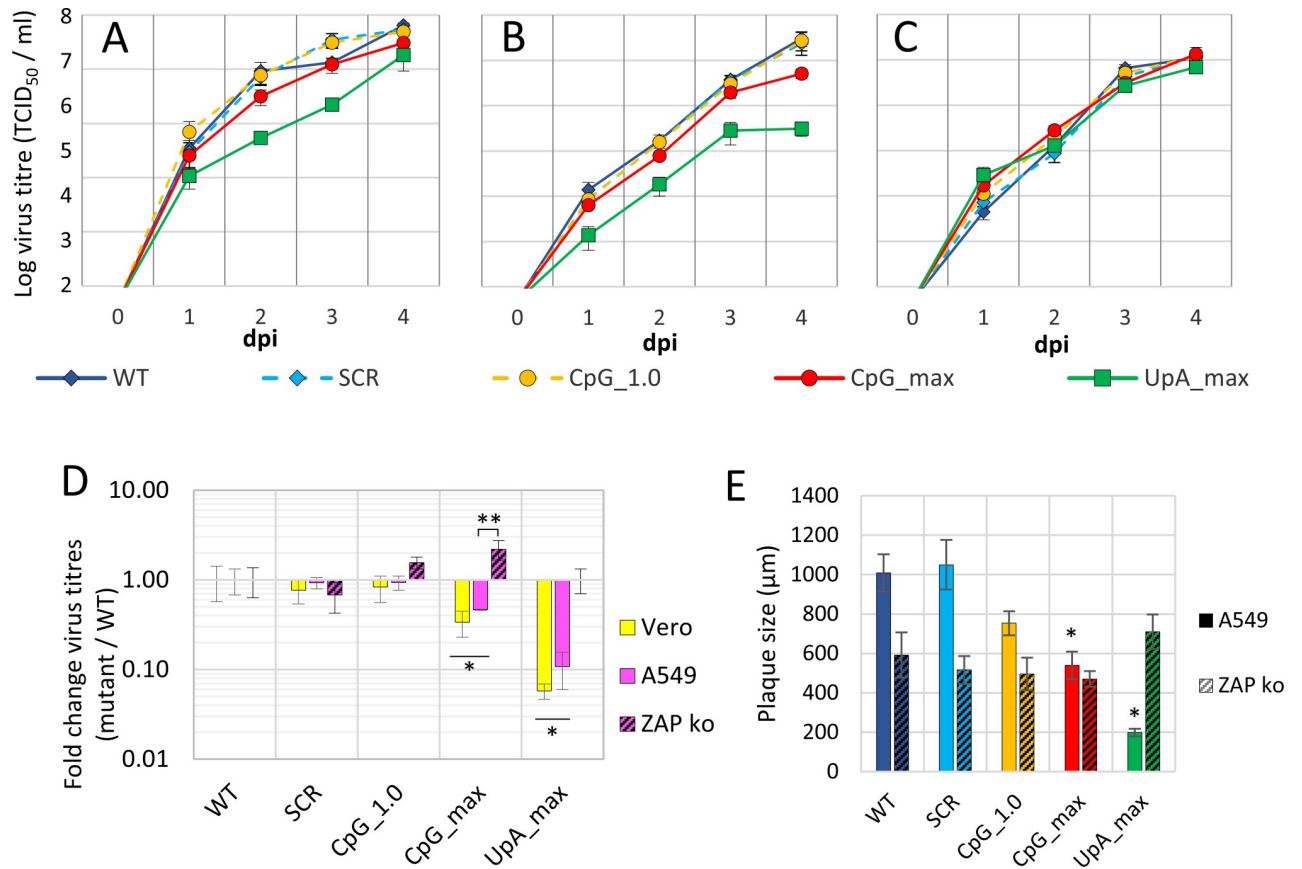


Fig 2. Replication of ZIKV with increased UpA and CpG dinucleotides is restricted in vertebrate cell culture. Vertebrate Vero E6 cells (A), A549 cells (B), and A549 ZAP knockout cells (C) were infected with the mutant ZIKV viruses at 1 RNA/cell. At the indicated dpi, the 50% tissue culture infectious dose was determined by end-point dilution assays. (D) Relative replication of mutant viruses was calculated by dividing mutant over WT virus titers at 2 dpi. Data points represent the average of a total of 4 independent experiments, compiled of 2 experiments performed for each of 2 independently rescued virus populations. The error bars indicate 1 standard error of the mean. Single asterisks highlight significant differences in WT vertebrate cells from WT ZIKV and 2 asterisks the difference between A549 cells and A549 ZAP knockout cells (two-way ANOVA, FDR adjusted $p < 0.05$). (E) Average plaque size measured in A549 and A549 ZAP knockout cells 3 dpi with ZIKV or indicated mutant viruses. After removal of the overlay, cells were fixed and stained for ZIKV E protein. Micrographs were taken from plaques from 2 independent experiments. The plaque diameter was measured using the Axiovision software. Data points represent the average plaque size, error bars indicate 1 standard error of the mean, and asterisks highlight significant difference from WT (one-way ANOVA with Dunnett's post hoc test, $p < 0.05$). Please refer to S1 Data for the numerical values underlying this figure. dpi, days postinfection; FDR, false discovery rate; ko, knockout; SCR, scrambled control virus; WT, wild-type; ZAP, zinc-finger antiviral protein; ZIKV, Zika virus.

<https://doi.org/10.1371/journal.pbio.3001201.g002>

significantly smaller average plaque sizes (530 μm and 200 μm , respectively) (Fig 2E and S1D Fig) (one-way ANOVA, $F(4, 23) = 19.06$, $p < 0.05$). The same virus dilutions were used to infect A549 ZAP knockout cells in parallel. In these cells, plaques observed in response to WT ZIKV infection were smaller compared to WT infections in ZAP expressing A549 cells. However, no further reduction in plaque sizes was observed when cells were infected with CpG- or UpA-high mutant ZIKV (Fig 2E and S1D Fig) (one-way ANOVA, $F(4, 19) = 1.020$, $p = 0.42$). Plaque phenotypes were confirmed in Vero E6 in which also the average plaque diameters of the CpG_1.0 mutant were significantly smaller than those of WT (S1E Fig) ($F(4, 25) = 65.29$, $p < 0.05$). The analysis of plaque diameters suggests that ZAP is responsible for the attenuation of both CpG_max and UpA_max mutant viruses. The results further suggest that the CpG_1.0 mutant is mildly attenuated in vertebrate cells that express ZAP, something that was not visible from the virus growth curves (Fig 2).

Replication of ZIKV mutants is differentially affected by genomic CpG and UpA dinucleotide frequencies in mosquito cells

Cell lines originating from *Aedes* spp. mosquitoes were infected with WT ZIKV and the mutant viruses to investigate how changes in CpG and UpA dinucleotide frequencies affect ZIKV replication in invertebrate cells. The replication kinetics of WT ZIKV and the SCR control were highly similar. Interestingly, both mutants with increased CpG dinucleotide frequencies (Fig 3A and 3B and S2A–S2C Fig, circles) displayed an increased fitness compared to WT in all *Aedes* mosquito cells tested, with a most consistent difference in the exponential growth phase at 2 days postinfection. Two days postinfection, the mean virus titers of the CpG_1.0 and the CpG_max mutants across all 5 cell lines were 6- and 5- fold higher than WT, respectively (two-way ANOVA, $F(4, 45) = 4.120$, $p < 0.05$). In contrast, virus titers of the UpA_max mutant were lower than WT in all cell lines tested; however, this did not significantly differ from WT (Fig 3C).

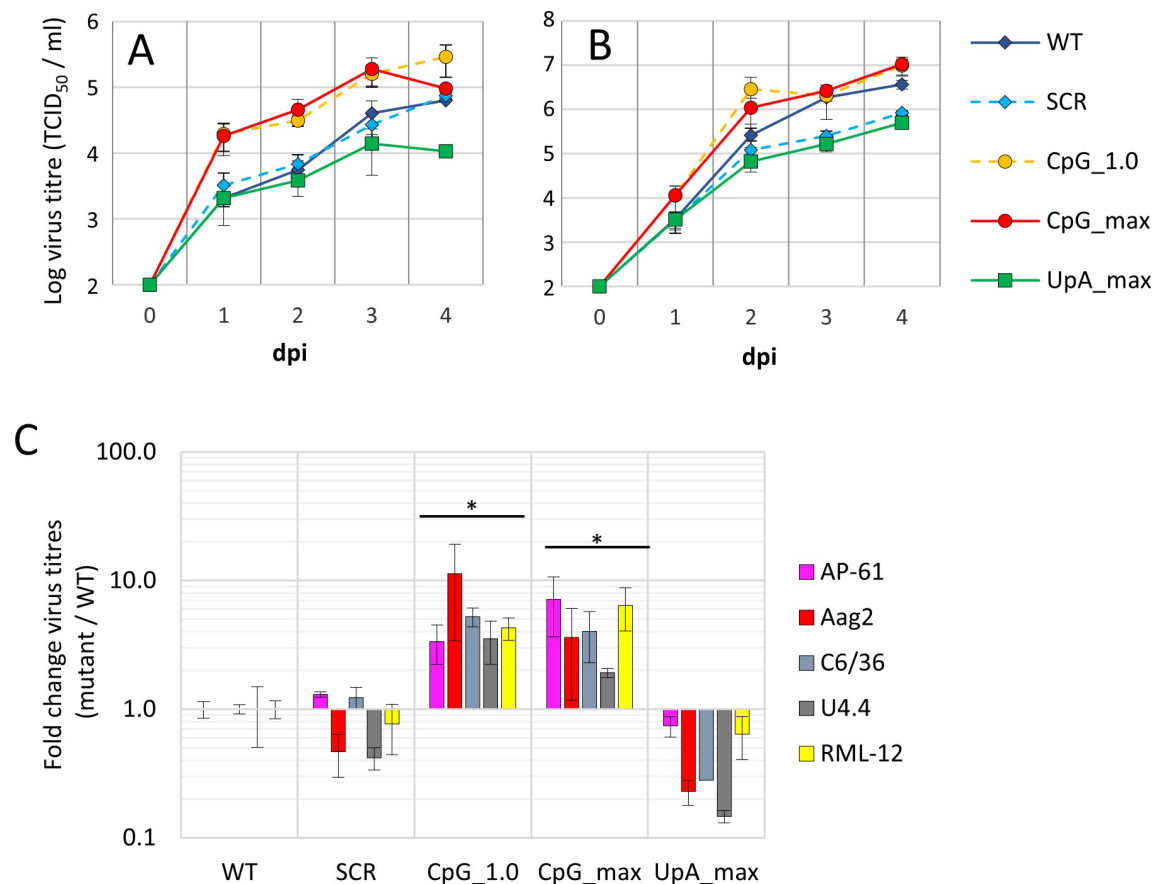


Fig 3. Replication of ZIKV with increased CpG dinucleotides has a replication advantage in mosquito cells. *Aedes* mosquito cells: *Ae. pseudoscutellaris* AP-61 (A) and *Ae. aegypti* Aag2 (B) were infected with the mutant ZIKV viruses at 10 RNA/cell. At the indicated dpi, the 50% tissue culture infectious dose was determined by end-point dilution assays. Data points represent the average of a total of 4 independent experiments, compiled of 2 experiments performed for each of 2 independently rescued virus populations. (C) Relative replication of mutant viruses in 5 distinct mosquito cell lines originating from *Ae. pseudoscutellaris* AP-61 (A), *Ae. aegypti* Aag2 (B), and *Ae. albopictus* RML-12, C6/36, and U4.4 (growth curves in S2 Fig) were calculated by dividing mutant over WT virus titers at 2 dpi. The error bars indicate 1 standard error of the mean. Numerical values for this figure are available in S1 Data. Asterisks indicate that over all 5 mosquito cell lines, mutant virus replication is significantly different from WT (two-way ANOVA, $F(4, 45) = 4.120$, FDR adjusted $p < 0.05$). dpi, days postinfection; FDR, false discovery rate; SCR, scrambled control virus; WT, wild-type.

<https://doi.org/10.1371/journal.pbio.3001201.g003>

To confirm the opposing replicative fitness of the CpG-high mutant viruses in either vertebrate or mosquito cells in a more sensitive assay, a competitive fitness experiment was performed. Human A549 cells, A549 ZAP knockout cells, and AP-61 mosquito cells were infected with 2 ZIKV variants. WT ZIKV was mixed with either the SCR, CpG-high viruses (CpG_1.0 and CpG_max), or UpA_max at equal RNA concentrations. Virus was passaged to new cells twice before total RNA was isolated and part of the mutated region within the ZIKV genome was reverse transcribed and PCR amplified. Amplicon DNA was digested to identify WT and mutant viruses. As expected, WT and SCR viruses were both detected in all 3 cell types (Fig 4A). In A549 cells, the CpG_1.0 mutant was almost eliminated, while the CpG_max mutant was completely outcompeted by WT (Fig 4B and 4C). In contrast, in AP-61 mosquito cells, more CpG_max ZIKV was detected compared to WT and the CpG_1.0 mutant had almost completely outcompeted WT (Fig 4B and 4C). The UpA_max mutant was outcompeted by WT in A549 cells, while in mosquito cells, it displayed fitness equal to that of WT. Knockout of ZAP strongly reduced any fitness advantages of WT over the mutants in A549 cells as all mutants were readily detected together with WT (Fig 4A–4D). Together with the virus growth curves, this indicates that while vertebrate cells attenuate the replication of viruses with increased CpG dinucleotide frequencies, these viruses have a replication advantage in mosquito cells.

CpG-high ZIKV is more infectious in *Aedes aegypti* mosquitoes

To investigate the biological role of dinucleotide frequencies in arbovirus RNA in living invertebrate vectors, *Aedes aegypti* mosquitoes were orally infected with WT ZIKV and the mutant viruses. Mosquitoes were fed an infectious blood meal containing a fixed number (10^8 /ml) of RNA copies, which for WT ZIKV equalled 5×10^5 TCID₅₀/ml (Fig 5). Engorged females were selected and incubated for 14 days before mosquito saliva was obtained. Whole body mosquito homogenates and saliva samples were scored for the presence of ZIKV (Fig 5A). Strikingly, 70% of the mosquito bodies became infected after ingesting CpG_1.0 ZIKV and 76% after ingesting the CpG_max ZIKV mutant, while this was only between 26% and 37% for mosquitoes that had ingested WT, SCR, or UpA_max viruses (Fig 5B).

Between 13% and 16% of mosquitoes carried infectious WT, SCR, or UpA_max ZIKV in their saliva. Significantly higher percentages of ZIKV-positive saliva were detected among mosquitoes that fed on blood containing the CpG_1.0 (50%) and CpG_max (52%) ZIKV mutants (Fisher exact test, $p < 0.01$) (Fig 5C). This indicates that dissemination into the saliva also occurred more frequently when mosquitoes were infected with the CpG-high viruses. Interestingly, a notable mortality of mosquitoes that fed on the CpG_max ZIKV mutant was observed during the experiment (log-rank test, $p < 0.001$) (Fig 5D). Despite the different infection rates, whole body homogenates of WT, SCR, CpG_1.0, and CpG_max ZIKV-infected mosquitoes contained similar viral titers (approximately 10^7 TCID₅₀/ml) (Fig 5E). However, mosquitoes infected with UpA_max ZIKV displayed 10-fold lower viral titers (Mann-Whitney U , $p < 0.05$) (Fig 5E). In an independent experiment in which mosquitoes were fed blood meals containing equal infectious virus titers (5×10^5 TCID₅₀/ml) instead of equal RNA copy numbers, mosquitoes were again more often infected with the ZIKV mutants with elevated CpG frequencies, compared to WT and SCR ZIKV (S4 Fig) (Fisher exact test, $p < 0.01$).

ZIKV mutants with elevated CpG and UpA dinucleotide frequencies show attenuated infection in IFNAR^{-/-} mice

To investigate the behavior of ZIKV mutants in a mammalian host, groups of adult male IFNAR^{-/-} mice (defective in the interferon- α/β receptor) were infected with the WT and

Fig 4. Fitness comparison between WT and mutant ZIKV in human and mosquito cells. Human A549 cells, A549 ZAP knockout cells, and AP-61 mosquito cells were infected with equal RNA concentrations of WT ZIKV mixed with either the SCR (A), CpG-high viruses (CpG_1.0 and CpG_max) (B, C), or UpA_max (D). Virus was passaged to new cells twice, before total RNA was isolated. ZIKV RNA was amplified with RT-PCR and digested with BsaI (A), Sali (B, C), or HeaIII (D) restriction enzymes to distinguish between WT and the respective mutant viruses. DNA gel images display the largest most distinctive products from each digestion. For more information, see S3 Fig. From left to right images display the digested DNA of the indicated individual viruses, followed by 2 independent experimental repeats performed with separately rescued virus populations (numbered 1 and 2). RT-PCR, reverse transcription PCR; SCR, scrambled control virus; WT, wild-type; ZAP, zinc-finger antiviral protein; ZIKV, Zika virus.

<https://doi.org/10.1371/journal.pbio.3001201.g004>

ZIKV mutants or were injected with PBS as a negative control (Fig 6A). Weight loss and viremia were determined for each animal. During the first 5 days, mice infected with WT or SCR ZIKV lost 6% to 8% of their total body weight (Fig 6B). Infections with the CpG_1.0 and CpG_max ZIKV mutants resulted in a 5% to 6% loss of total body weight. However, the mice infected with the CpG_1.0 and CpG_max ZIKV mutants recovered faster than mice infected with WT ZIKV and reached their respective initial body weights around days 23 and 29 post-infection compared to 32 dpi for mice infected with WT ZIKV. Mice that were inoculated with UpA_max ZIKV or PBS showed no signs of disease and maintained a healthy body weight throughout the experiment (Fig 6B). Next, blood viremia levels in mice infected with both mutants that displayed reduced weight loss were compared to those infected with WT ZIKV. Mice infected with the CpG_max and UpA_max ZIKV mutants still developed substantial viremia, which was detected for 7 days postinfection. However, at peak viremia, titers were on average 5-fold lower than for WT ZIKV (Fig 6C, day 3). All infections resulted in strong anti-ZIKV immunoglobulin G (IgG) antibody responses in week 4, though responses in CpG_max and UpA_max infected mice led to mildly lower (approximately 2-fold) end-point ELISA titers compared to infections with WT, SCR, and CpG_1.0 ZIKV (Fig 6D) (one-way ANOVA, $F(4, 20) = 6.917, p < 0.05$).

Challenge with ZIKV_{PRVABC59}

The mice were subsequently challenged with ZIKV_{PRVABC59} on day 32 after the immunizing infection, with the ZIKV mutants (see Fig 6A). All the previously infected mice were protected against ZIKV_{PRVABC59}-induced weight loss (Fig 7A). Only those mice that were mock infected with PBS showed signs of weight loss and developed ZIKV viremia after the challenge (Fig 7A and 7B). In this IFNAR^{-/-} mouse model, ZIKV infection results in testicular damage, clearly seen as substantial overt reductions in testis size. The unvaccinated PBS control group displayed a marked reduction in testis size after challenge with ZIKV_{PRVABC59}. Testis size reductions were also observed in mice immunized with WT ZIKV and the SCR and CpG_1.0 ZIKV mutants, likely as a result of the first infection rather than due to ZIKV_{PRVABC59} challenge, given that all mice seroconverted after the initial infection (Fig 6D). Mice that were first infected with the CpG_max and UpA_max ZIKV mutants retained normal testis size after challenge with ZIKV_{PRVABC59} (Fig 7C) (Kruskal-Wallis test, $p < 0.05$), illustrating that neither the first infection nor ZIKV_{PRVABC59} challenge resulted in detectable testes damage. The suitability of using these 2 mutants as a vaccine was further evaluated by infecting additional mice with either CpG_max or UpA_max ZIKV mutants, with the size of their testes determined 49 days postinfection. No reduction in testes size was observed when compared to noninfected (naïve) mice (Fig 7D). Real-time quantitative reverse transcription PCR (qRT-PCR) of the testes also illustrated that neither CpG_max nor UpA_max ZIKV mutants contained detectable levels of ZIKV RNA (Fig 7E). Together, these results indicate that the CpG_max and UpA_max ZIKV mutants do not cause testes damage and can protect against ZIKV challenge.

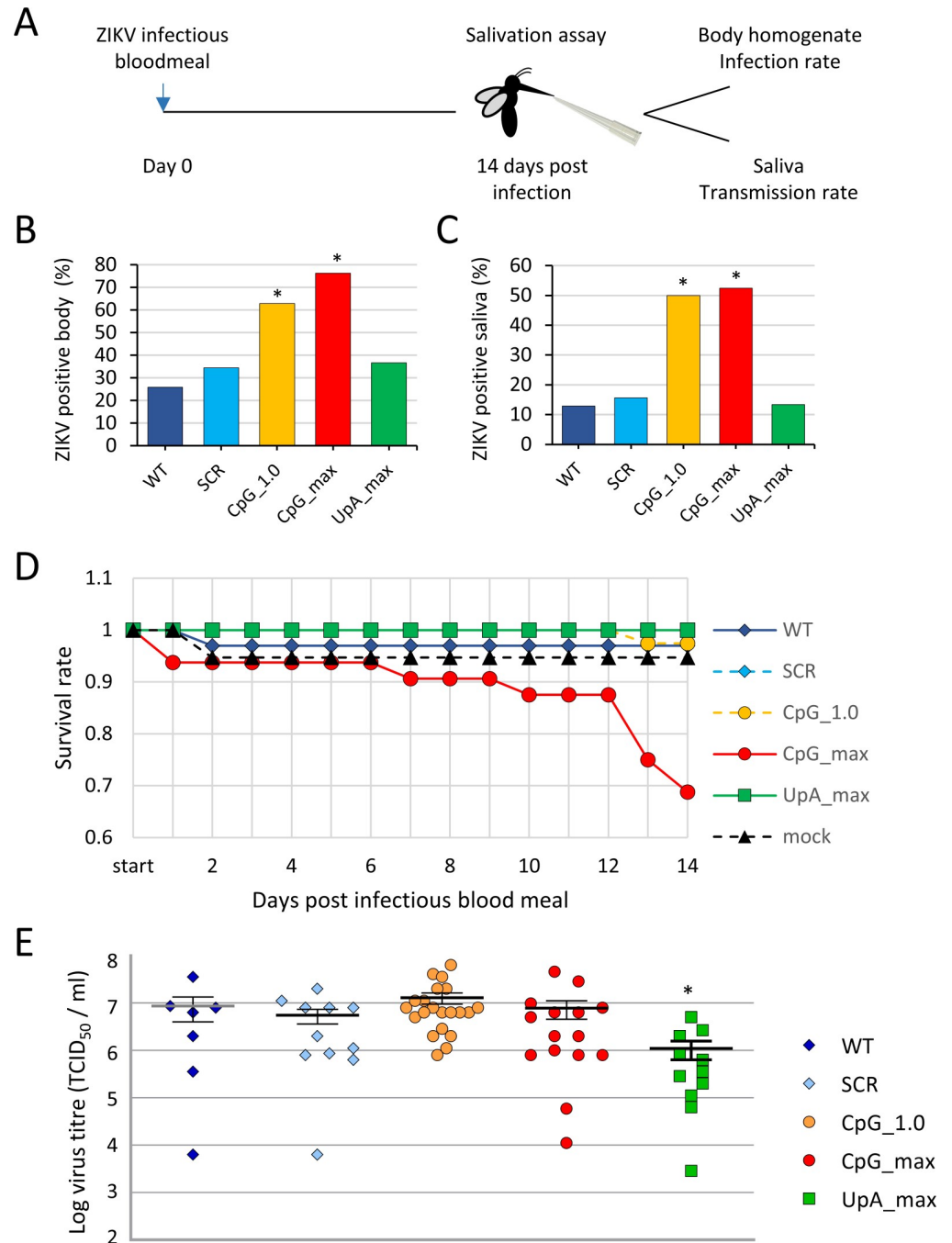


Fig 5. Infection of *Aedes aegypti* with ZIKV mutants. *Aedes* mosquitoes were offered an infectious blood meal containing equal RNA concentrations of each of the ZIKV. Fully engorged females were selected and 14 days later subjected to a salivation assay (A). Mosquito body homogenates (B) and mosquito saliva (C) were inoculated on Vero E6 cells to detect the presence of infectious virus. Bars represent the percentage of ZIKV-positive samples with n between 21 and 36 engorged mosquitoes per experimental group. Asterisks represent significant difference from WT (Fisher exact test, $p < 0.01$). Survival rate of blood-fed mosquitoes during the experiment was differentially affected by mutant viruses (log-rank test, $p < 0.001$), with n between 31 and 39 mosquitoes that had engorged an infectious blood meal at the start of the experiment (D). The infectious virus titer inside ZIKV-positive mosquito bodies was determined by end-point dilution assays. Data points indicate individual mosquito samples and the mean and SEM for each experimental group are displayed. Asterisk indicates significant difference from WT (Mann-Whitney U, $p < 0.05$) (E). Please refer to S1 Data for the numerical values underlying panels B–E. SCR, scrambled control virus; WT, wild-type; ZIKV, Zika virus.

<https://doi.org/10.1371/journal.pbio.3001201.g005>

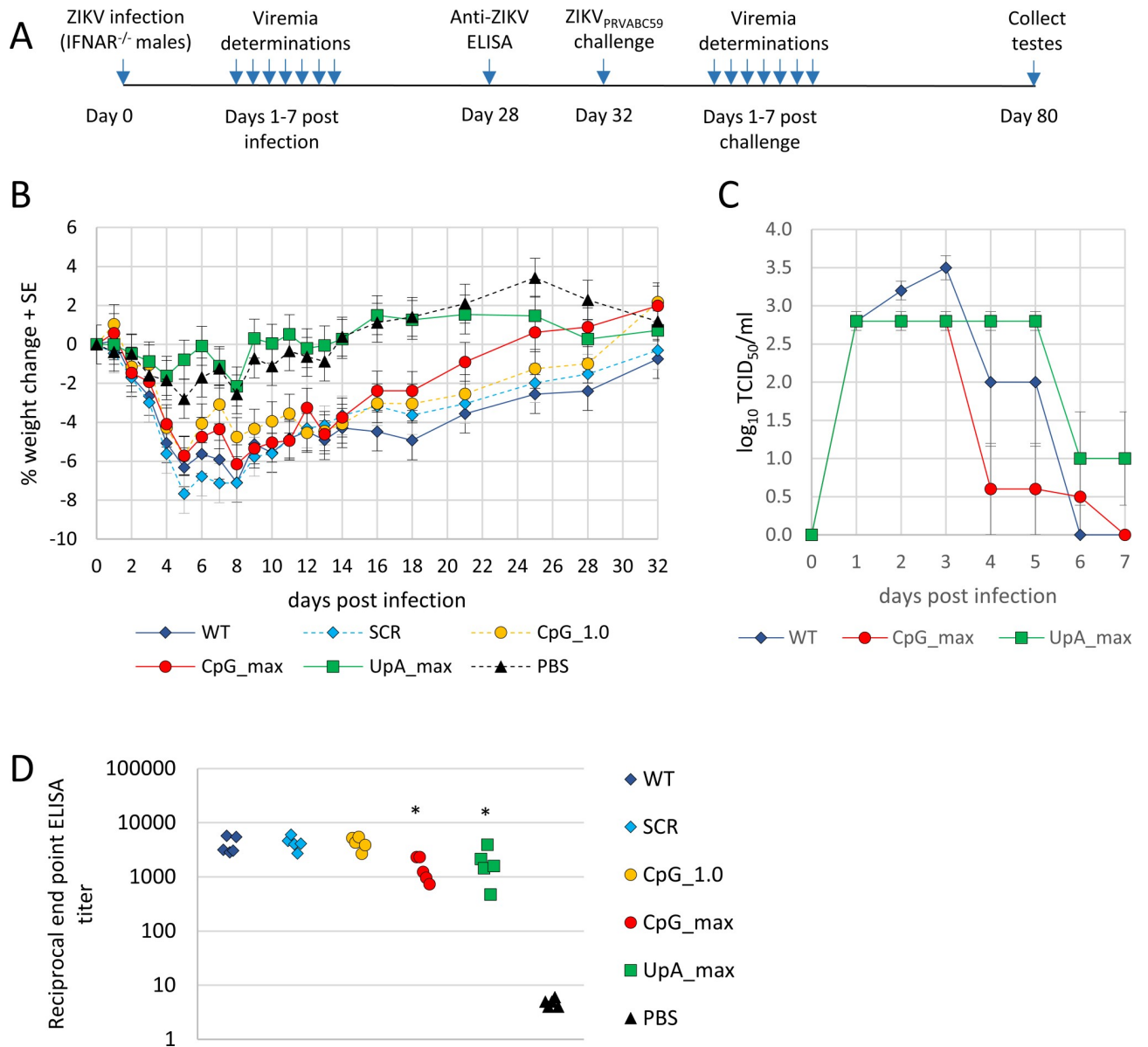


Fig 6. Weight loss, viremia, and ZIKV antibody responses postprimary ZIKV infection. (A) Timeline of experiment. (B) Weight loss of IFNAR^{-/-} mice postinfection (*n* = 5 mice per group). (C) Viremia postinfection of mice infected with WT ZIKV or CpG_{max} or UpA_{max} ZIKV. (D) 50% End-point of total IgG ELISA titers 4 weeks postvaccination with indicated ZIKV mutants. Significant changes from WT are calculated by a one-way ANOVA with Dunnett multiple comparisons test and indicated with asterisks (*p* < 0.05). Numerical values for panels B–D are available in [S1 Data](#). IgG, immunoglobulin G; SCR, scrambled control virus; WT, wild-type; ZIKV, Zika virus.

<https://doi.org/10.1371/journal.pbio.3001201.g006>

Discussion

The motivation for this study was the evident difference in CpG dinucleotide representation in the genomes of RNA viruses infecting vertebrates compared to those infecting insects (Fig 1) [5,13,14,31]. A recent study reported that ZIKV mutants with elevated CpG dinucleotide frequencies were attenuated in vertebrate cells and mice, while no significant effects on virus replication were observed in C6/36 *Aedes albopictus* cells [36]. This suggests that CpG suppression in arbo flaviviruses is required for sufficient replication in vertebrate hosts and that there is no selection on CpG dinucleotide frequencies in mosquitoes or other arthropod hosts.

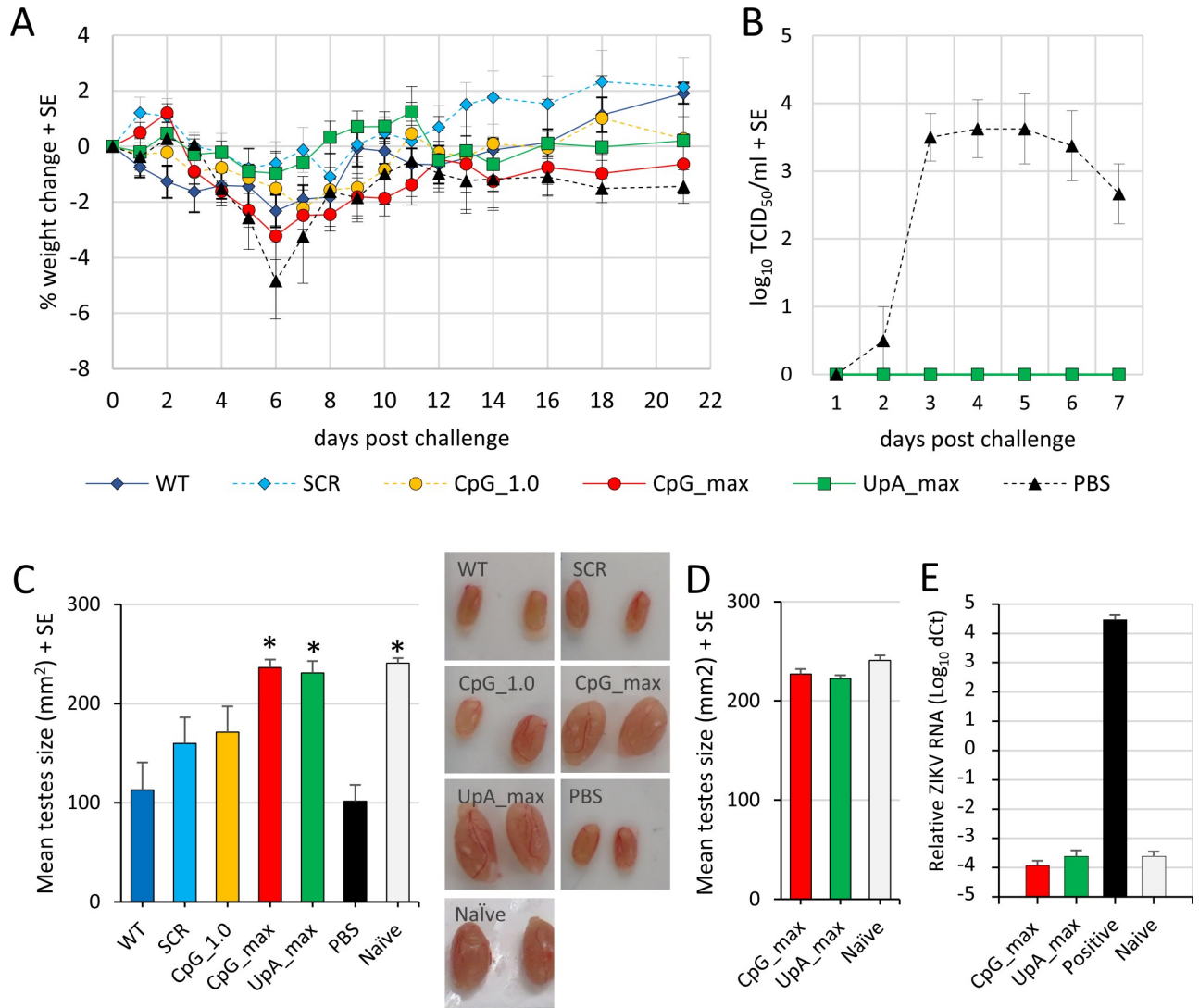


Fig 7. Weight loss, viremia, and testes size in *IFNAR*^{-/-} mice post-ZIKV_{PRVABC59} challenge. (A) Weight loss of ZIKV_{PRVABC59}-challenged *IFNAR*^{-/-} mice (*n* = 3–5 mice per group). (B) Viremia post-ZIKV_{PRVABC59} challenge (*n* = 4–5 mice per group). (C) Testes size (height × width) and representative images of testes from vaccinated mice post-ZIKV_{PRVABC59} challenge compared with testes of not vaccinated, PBS-injected control mice and naïve (uninfected, healthy control) mice. Asterisk indicates significant difference from mice that received PBS injections instead of vaccination prior to ZIKV_{PRVABC59} challenge (Kruskal–Wallis test, *p* < 0.05). (D) Vaccine safety test displays the mean testis size of mice infected with CpG_{max} or UpA_{max} mutant viruses (*n* = 6 mice per group, testes harvested on day 49 postvaccination) compared with testes size of naïve mice (*n* = 3) without subsequent challenge. (E) qRT-PCR of ZIKV RNA in testes of mice from D and mice infected with ZIKV_{PRVABC59} for 48 days as positive control. Bars represent the mean Ct values normalized for RPL13A housekeeping RNA. The numerical values for this figure are available in *S1 Data*. Ct, cycle threshold; qRT-PCR, real-time quantitative reverse transcription PCR; SCR, scrambled control virus; WT, wild-type; ZIKV, Zika virus.

<https://doi.org/10.1371/journal.pbio.3001201.g007>

However, in our experiments, ZIKV mutants with elevated CpG dinucleotide frequencies (CpG representations of 1.0 and 1.62) reproducibly showed enhanced replication rates in a range of different *Aedes* spp. mosquito cell lines (Fig 3). Importantly, live vector mosquitoes became more frequently infected with the CpG-high ZIKV mutants and dissemination into the saliva occurred more often compared to infections with WT ZIKV (Fig 4). In marked contrast to these proviral effects of increased CpG frequencies, elevated UpA dinucleotide frequencies resulted in reduced replication rates in mosquito cell cultures and lowered virus titers in infected *Ae. aegypti* mosquitoes (Figs 3 and 4). Taken together, this study provides the first

experimental evidence that dinucleotide composition of viral genomes is subject to substantial evolutionary pressures in invertebrate mosquito cells.

This new information sheds light on the biological basis for the compositional differences between flaviviruses that are arthropod-borne and those that replicate exclusively in arthropod hosts (ISFs). Both groups of flaviviruses persistently infect their arthropod hosts without any noticeable pathogenicity. The observation that elevated CpG frequencies enhance ZIKV replication in mosquito cells (Figs 3 and 4) suggests that WT ZIKV infections in mosquitoes are normally attenuated. The substantial mortality in mosquitoes infected with the CpG_max ZIKV (Fig 4D) further illustrates how finely balanced CpG composition has to be maintained for flaviviruses to persistently infect their arthropod hosts, especially given that the mutated region represents only 15% of the ZIKV genome. Lineage 2 ISFs mildly suppress CpG dinucleotides (Fig 1) and are believed to have evolved from arboviruses that lost the ability to infect vertebrate cells [31]. Rather than drifting toward an unbiased CpG dinucleotide frequency due to a lack of selection pressure, the observed evolutionary pressures in mosquito cells suggest that lineage 2 ISFs accumulate CpG dinucleotides by natural selection. However, the accumulation of CpG dinucleotides in lineage 2 ISF genomes is potentially constrained as nonpathogenic persistent replication needs to be maintained.

This delicate balance additionally has to be sustained in the context of antiviral responses. In the arthropod host, the most potent antiviral responses are mediated through RNAi (reviewed in [37]). Suppression of RNAi in mosquitoes infected with Sindbis virus (arbovirus from family *Togaviridae*, genus *Alphavirus*) results in increased mosquito mortality [38]. However, replication of the ZIKV mutants with elevated CpG or UpA dinucleotide frequencies was similarly enhanced or suppressed, respectively, in all mosquito cells tested, including C6/36 cells (Fig 3), which are defective in the production of antiviral siRNAs [39,40]. This suggests that other pathways or mechanisms are active in discriminating dinucleotide frequencies in mosquitoes.

Alternatively, synonymous changes in dinucleotide frequencies inevitably alter the codon usage of a nucleotide sequence and changes in translation efficiency may affect the biosynthesis rate of the encoded viral polyprotein and as a consequence viral replication rates. However, comparison of the synonymous codon usage of the mutated region in ZIKV and the synonymous codon frequency of human and insect reference sets show no consistent correlation between the elevation of CpGs and similarities in codon usage with either host reference set (S1 Table). Indeed, previous studies have largely discounted effects of codon use or codon pair bias as the explanation for attenuation of CpG-high mutants of vertebrate viruses. For example, elevation of CpG and UpA dinucleotide frequencies in untranslated regions of viral RNA attenuated virus replication to equivalent degrees as similar dinucleotide modifications in coding regions of the viral genome [15,16,41]. Furthermore, it is now established that the vertebrate antiviral protein ZAP mediates the attenuated replication of viruses with high CpG frequencies.

In vertebrates, the N-terminal zinc-fingers of ZAP bind high CpG containing RNA sequences through a number of hydrogen bonds and stacking interactions [22] to initiate a plethora of downstream intracellular interactions with proteins involved in translation, RNA degradation, and antiviral immunity [20,23–28,42]. Specifically, the host proteins RNaseL, activated by OAS3, and both TRIM25 and KHNYN are crucial for the ZAP-mediated attenuation of CpG-high E7 and HIV-1, respectively [16,21,29]. Correspondingly, knockout of ZAP or OAS3/RNaseL abolished the attenuated phenotype of ZIKV mutants with elevated CpG dinucleotide frequencies in vertebrate cells (Fig 2). Additionally, mice vaccinated with CpG_max ZIKV and subsequently challenged with ZIKV_{PRVABC59} did not show any signs of ZIKV-induced testicular damage as measured by their testis size, whereas vaccination with

CpG_1.0 ZIKV resulted in an intermediate reduction in average testis size (Figs 6 and 7). Together, these results indicate that the degree of virus attenuation is correlated to CpG composition and mediated by vertebrate ZAP.

While most recent investigations involving genome composition and virus replication have focussed on CpG dinucleotides, a growing body of evidence indicates a substantial additional effect of UpA dinucleotide frequencies on virus attenuation. UpA dinucleotides are suppressed in vertebrate and invertebrate animals and their viruses (Fig 1) [14]. The UpA_max ZIKV mutant used in this study showed strong attenuation in vertebrate cells and no signs of disease in mice (Figs 2 and 6). Moreover, the attenuated phenotype of UpA_max ZIKV was rescued by knockout of ZAP, suggesting that the interaction between ZAP and UpA dinucleotides is not exclusive for previously published E7 mutant viruses [21]. Whether ZAP directly binds UpA dinucleotides or requires additional host proteins for this interaction is unknown and remains a topic of active investigation [43]. Whether the selection against UpA dinucleotides in insect cells is equally strong as that observed in vertebrate cells remains unclear. Although flaviviruses suppress UpA dinucleotides in their RNA, UpA_max ZIKV replication and dissemination was not consistently reduced compared to WT ZIKV in mosquito cells and live mosquitoes, respectively (Figs 3–5).

The diverse selective pressures that arboviruses encounter have influenced arbovirus disease emergence on multiple levels (reviewed in [44]). The current study identifies CpG frequencies as a key adaptive trait that enables ZIKV to replicate in 2 profoundly different hosts. Furthermore, the finding that increasing CpG frequencies enhanced the replication of ZIKV in mosquitoes provides evidence that CpG frequency differences between vector-borne flaviviruses and ISFs do not simply result from compositional constraints in one host and none in the other. Instead, the data indicate the existence of strongly conflicting evolutionary pressures on ZIKV to enable sufficient replication in both hosts to maintain a vector-borne life cycle. In contrast to flaviviruses, vector-borne viruses from the genus *Alphavirus* contain relatively high CpG dinucleotide frequencies, which may suggest these viruses have evolved a more optimal genome composition for replication in the mosquito vector. Although most alphaviruses effectively infect vertebrate cells, these viruses are highly sensitive to ZAP [45]. The same constraints may operate in other dual-host viruses. For example, we and others recently discovered that the replication of potato virus Y and plum pox virus (genus *Potyvirus*) in plants was similarly attenuated by the synonymous introduction of CpG and UpA dinucleotides [46,47]. Plant transcriptomes also display CpG suppression that is also reflected in the majority of plant RNA viruses. This suggests that plant viruses which are maintained in transmission cycles involving persistent replication in both plant host and arthropod vectors [48] may encounter similarly conflicting evolutionary pressures as arboviruses.

The findings can spark investigations into novel strategies to intervene with the transmission cycles of arboviruses. Attenuating vertebrate viruses by increasing CpG and UpA dinucleotide frequencies is a promising and universally applicable approach to generate live-attenuated virus vaccines (Figs 6 and 7) [17,36]. The enhanced replication of CpG-high mutants of ZIKV in mosquito cells may serve to improve production of live-attenuated or inactivated vaccines and can lead to novel immunization strategies [49]. A radical, yet intriguing application is to release CpG-high infected mosquitoes into the environment to serve as vaccine vectors. At the moment, this application remains purely hypothetical as such an approach raises many questions regarding ethics, vaccine safety, and the spread of genetically modified viruses into the environment. However, theoretically mosquitoes could be highly effective (Fig 5) in not only vaccinating humans and livestock but also animal reservoirs by transmitting high doses of flavivirus vaccines with the same attenuated replication in vertebrate animals as observed in the experimentally infected mice (Figs 6 and 7).

Materials and methods

In silico analyses

A single full-length flavivirus genome was selected per flavivirus species. For analysis of host gene composition, mRNA sequences of human (GRCh38.p13i) and *Ae. aegypti* (AaegL5.0) were downloaded from RefSeq (<https://www.ncbi.nlm.nih.gov/nucore>). From these datasets, representative selections of 10,000 sequences were extracted at random using Perl with an in-house script. Sequences were filtered to exclude coding region sequences of length <250 bases. To avoid redundancy, similar or identical sequences (<1% nucleotide divergence) were identified with SSE software (v1.4) [50] and removed from the dataset. This resulted in over 9,000 human and mosquito sequences, which were used for composition analysis (all GenBank accession numbers available in [S1 Text](#)). Dinucleotide frequencies were calculated using the program Composition Scan within SSE (v.1.4). Synonymous site variability (SSV) and MFED of the ZIKV genome were calculated as previously described, using a fragment size of 200 and sliding window of 21 codons for SSV and a fragment size 200 with 48 nucleotide increments for MFED using a selection of ZIKV isolates [51]. The codon adaptation index (CAI) of full length ZIKV and the mutated regions was calculated using an online CAI calculator (www.biologicscorp.com) with the codon usage of *H. sapiens* and *Drosophila melanogaster* as reference data sets ([S1 Table](#)).

Cells and viruses

Ae. albopictus C6/36 (ATCC CRL-1660) and U4.4 were cultured at 28°C in Leibovitz-L15 medium (Gibco, Carlsbad, California, United States of America) supplemented with 10% heat-inactivated fetal bovine serum (FBS; Gibco), 2% tryptose phosphate broth (Gibco), and 1% non-essential amino acids (Gibco). *Ae. albopictus* RML-12 cells were cultured in Leibovitz's L-15 medium supplemented with 10% FBS and 10% tryptose phosphate buffer at 28°C [52]. *Ae. aegypti* Aag2 cells [53] and *Ae. pseudoscutellaris* AP-61 cells [54] were cultured at 28°C in Schneider's *Drosophila* medium (Gibco) supplemented with 10% FBS. Human A549 cells including ZAP, RNaseL, 2'-5'-oligoadenylate synthetase 1 (OAS1), and OAS3 knockout cells were described previously [21], and African green monkey kidney Vero E6 (ATCC CRL-1586) were all maintained at 37°C with 5% CO₂ in Dulbecco's modified Eagle medium (DMEM) (Gibco) supplemented with 10% heat-inactivated FBS, 100 U/ml penicillin, and 100 µg/ml streptomycin (Sigma-Aldrich, Zwijndrecht, The Netherlands). Cell lines were routinely checked for mycoplasma using MycoAlert Mycoplasma Detection Kit (Lonza, Breda, The Netherlands).

A pCC1-BAC-based and SP6 promoter-driven infectious clone of the ZIKV_{BeH81901} isolate from Brazil (GenBank KU365778.1) [55] was used for the construction of mutant viruses. A region of 1,653 nucleotides was selected for the described synonymous mutations. Mutant regions with elevated CpG or UpA dinucleotide frequencies were designed using the "mutate sequence" function in SSE, taking care not to alter the coding amino acid sequence or the other UpA or CpG dinucleotide, respectively. The SCR sequence was originally designed for a region of 4,344 nucleotides that included the above mentioned mutated region using the "scramble sequence" function in SSE with the CDLR algorithm. The amino acid sequence, codon usage, and dinucleotide usage of the SCR sequence were kept identical to that of the corresponding WT sequence. Mutated regions were synthesized (Geneart, Thermo Fisher Scientific, Regensburg, Germany) and incorporated into the viral genome using unique restriction sites RsrII and BstBI (New England Biolabs, Ipswich, United States). Nucleotide sequences of mutated regions are listed in [S2 Text](#). Plasmid DNA was linearized with PmeI (New England Biolabs) and complete digestion was verified on agarose gel. Linearized DNA was purified by phenol/chloroform extraction and RNA was in vitro transcribed in the presence of G(5')ppp(5')G RNA Cap

structure analog using SP6 polymerase (New England Biolabs) according to the manufacturer's protocol. RNA was transfected into Vero cells with lipofectamine 2000 (Invitrogen, Carlsbad, United States) to launch virus replication. Between 1 and 4 days posttransfection, cytopathic effects were observed and cell culture supernatant was transferred to a fresh 60% confluent monolayer of Vero cells to generate passage 1 (P1). After 2 hours, inoculum was removed and cells were washed with cell culture medium. Three days postinfection, cell culture supernatant was harvested. Newly generated mutant virus stocks were sequence verified by reverse transcriptase PCR (see competition assay below for details) followed by restriction analysis using DdeI, Sall, and PstI restriction enzymes (New England Biolabs) and DNA sequencing (Macrogen Europe, Amsterdam, The Netherlands). Stocks were again verified by restriction digestion prior to the mouse experiments. At the end of the mosquito experiments, total RNA from pools of 8 infected mosquitoes was isolated and ZIKV mutants were sequence verified by RNA-sequencing (BGI Genomics, Beijing, China) as described previously [56].

Virus quantification

Tissue culture infectious dose 50% (TCID₅₀) was determined by end-point dilution assays (EPDA). Serial 10-fold dilutions of virus stocks and experimental samples were prepared in complete DMEM cell culture medium. Vero E6 cells from confluent tissue cultures were detached with Trypsin-EDTA (Gibco) and dissolved in a total volume equal to 1 ml/1.67 cm². Cell suspension was added to the virus dilutions in a 1:1 ratio, mixed and plated in 6-fold onto microtiter plates (Nunc, Sigma-Aldrich, Zwijndrecht, The Netherlands). Virus titers were determined by CPE at the end-point of infection. For each of the mutant viruses, the viral titers determined by CPE and respective end-points of the EPDA were confirmed by immunofluorescence. Cells were washed with phosphate buffered saline (PBS) and fixed with 4% paraformaldehyde in PBS. ZIKV envelope was stained with 4G2, a pan-flavivirus primary α -E mouse monoclonal antibody diluted in PBS containing 2% FBS (1:50) [57] for 1 hour at 37°C. Samples were washed 3 times with PBS and stained with a secondary goat α -mouse Alexa Fluor 488 (1:2,000; Invitrogen). RNA copy numbers in virus stocks were determined by comparing RNA from virus stocks with purified SP6 in vitro transcribed RNA. RNA isolation was performed with TRIzol reagent for liquid samples according to the manufacturer's protocol. Reverse transcriptase and a real-time PCR were performed with 2 sets of ZIKV-specific primers F1 5'-cctgatgaccatctgtggca-3', R1 5'-cccatagagcaccactctt-3', and F2 5'-tcaggagtggtggtt-gaagg-3', R2 5'-gtgcccttctccatttgggt-3' using superscript III (Invitrogen) and SYBR green (Applied Biosystems, Waltham, United States) according to the respective manufacturer's protocols with an annealing temperature of 58°C during real-time PCR in a CFX96 real-time system (Bio-Rad, Hercules, United States) thermocycler.

Virus growth curves

Cell monolayers were seeded in 6-well plates to a 50% to 60% confluency. The cell culture fluid was removed and infections were performed by diluting virus stocks (P2) in standard culture media for each of the respective cell types in a total volume of 1 ml/well. After 2 hours, the inoculum was removed and the monolayers were washed twice with 1 ml of PBS, before 2 ml of fresh culture medium was added. At indicated times postinfection, 50 μ l of cell culture supernatant was taken per well and stored at -80°C until TCID₅₀/ml was determined by EPDA.

Competition assay

Equal concentrations of WT and mutant virus (1 RNA/cell) were mixed in DMEM or XXX cell culture medium and added to A549, A549 ZAP knockout, or AP-61 mosquito cells at 50%

confluence. After 2 hours, the inoculum was replaced with culture medium. Ten μl of cell culture supernatant was passaged to fresh cells. After 2 passages, total RNA was isolated using TRIzol reagent according to the manufacturer's protocol. RNA was reverse transcribed and part of the mutated region within the ZIKV genome was PCR amplified using SuperScript III One-Step RT-PCR System with Platinum Taq Polymerase (Invitrogen) together with either the 5'-aagtgagaaaaagatggg-3' (WT and SCR) or 5'-gaggaaaaagatggaagac-3' (WT, CpG_1.0, CpG_max, and UpA_max) forward primers in combination with a 5'-gtgccctttctcatttgg-3' reverse primer. Reverse transcription and PCR amplification were performed according to the manufacturer's protocol with the reverse transcription at 50°C for 30 minutes and an annealing temperature during PCR amplification of 58°C in an Applied Biosystems 2720 thermocycler. The resulting DNA amplicons from the comparisons between WT and SRC were digested with BsaI-HFv2 (New England Biolabs), WT and CpG_1.0 or CpG_max with SallI-HF (New England Biolabs) and WT and UpA_max with HaeIII (Invitrogen) and ran on 2% agarose gels.

Mosquito rearing

Ae. aegypti mosquitoes (Rockefeller strain, Bayer AG, Monheim, Germany) were maintained at $27 \pm 1^\circ\text{C}$ with 12:12 light:dark cycle and 70% relative humidity (RH). Adult mosquitoes were provided with 6% ad libitum glucose solution. Human blood (Sanquin Blood Supply Foundation, Nijmegen, the Netherlands) was provided through Parafilm using the Hemotek PS5 feeder (Discovery Workshops, Lancashire, United Kingdom). Adult mosquitoes were kept in Bugdorm-1 insect rearing cages ($30 \times 30 \times 30$ cm, Bugdorm, Taiwan, China) until they were 2 to 6 days old, before females were transferred to buckets (diameter: 12.2 cm, height: 12.2 cm; Jokey, Wipperfurth, Germany). Buckets contained approximately 50 females each and were transported to the Biological Safety Level 3 facility for virus infection assays.

Infectious blood meal

Virus solutions were made by diluting the virus stocks to equal concentrations in DMEM before mixing with human blood to their final concentrations. Infectious blood meals were offered through Parafilm using the Hemotek PS5 feeder. Mosquitoes from a single bucket were offered a single blood meal containing one of the ZIKV mutants and allowed to feed for 1 hour ad libitum in light conditions, at 24°C and 70% RH. Mosquitoes were anesthetized with 100% CO₂ and fully engorged females were selected. Engorged mosquitoes were kept for 14 days on glucose solution at 28°C in a 12:12 light:dark cycle.

Salivation assay

Fourteen days post blood meal, mosquitoes were anesthetized with 100% CO₂ and placed on a CO₂ pad. Mosquitoes that died within the 14 days incubation period were counted and discarded. Mosquitoes were immobilized by removing their legs and wings. The proboscis of each mosquito was inserted into a 200- μl yellow pipet tip (Greiner Bio-One, Kremsmünster, Austria) containing 5 μl of a 1:1 solution of 50% glucose solution and FBS, for 1 hour. After salivation, the mosquito bodies were added to 1.5 ml Safe-Seal micro tubes (Sarstedt, Nümbrecht, Germany) containing 0.5 mm zirconium beads (Next Advance, Averill Park, New York, USA). Each saliva sample was added to a 1.5-ml micro tube (Sarstedt) with 55 μl DMEM cell culture medium containing FBS, Penicillin and streptomycin supplemented with additional Fungizone (50 $\mu\text{g/ml}$; Invitrogen), and Gentamycin (50 $\mu\text{g/ml}$; Life Technologies, Bleiswijk, The Netherlands), hereafter referred to as DMEM-complete. Mosquito bodies and saliva samples were stored at -80°C until further processing.

Infectivity assays

Frozen mosquito bodies were homogenized for 2 minutes at speed 10 in a Bullet Blender Storm (Next Advance, Troy, United States). Homogenized bodies were centrifuged briefly and resuspended in 100 μ l DMEM-complete medium. Homogenization was repeated and mixtures were centrifuged for 1 minute at 14,500 rpm in a table top centrifuge. From the mosquito homogenates or thawed saliva samples, 30 μ l was used to inoculate a Vero cell monolayer in a 96-well plate. After 2 to 3 hours, the inoculum was removed and replaced with 100 μ l DMEM-complete. Wells were scored for virus induced CPE at 3 and 4 dpi. Bodies and saliva samples of infected mosquitoes were additionally titrated by EPDA.

Immunostained plaque assays

An 80% confluent monolayers of cells were infected with a series of 10-fold dilutions with equal RNA copies of each of the mutant viruses. After 2 hours of incubation, the inoculum was removed and a 1% carboxymethyl cellulose overlay was added. At the end of the experiment, the overlay was removed and cells were fixed and stained for ZIKV envelope protein using 4G2 primary antibodies and green Alexa Fluor 488 secondary fluorophores. Micrographs were taken with an Axio Observer Z1m inverted microscope in combination with an X-Cite 120 series lamp and AxioVision software of all primary plaques at the lowest possible concentration.

Infection of IFNAR^{-/-} male mice with mutant ZIKVs

All viruses were grown in C6/36 cells and titers were determined by immunostained TCID₅₀ assays using C6/36 cells. Briefly, virus was titrated in 10-fold serial dilutions in 96-well plates with C6/36 cells (2×10^4 cell/well). After 5 days, plates were washed and fixed in 80% cold acetone for 1 hour at -20°C . Acetone was removed. Plates dried and ZIKVs were detected by indirect immunofluorescence using mouse anti-4G2 monoclonal primary antibody and polyclonal goat anti-mouse IgG conjugated IRDye 800CW secondary antibody (LiCor, 926–32210). Staining was visualized using the LI-COR Biosciences Odyssey Infrared Imaging System and application software. Any staining in any well was considered positive and TCID₅₀ titers determined.

Male type I IFN receptors knockout (IFNAR^{-/-}) mice (C57BL/6J background) ($n = 5$ per group, age 2 to 6 months) were infected subcutaneously (s.c.) at the base of the tail with 10^3 TCID₅₀ (100 μ l in Roswell Park Memorial Institute (RPMI) 1640 supplemented with 2% FCS) of each virus per mouse. Mice were weighed at the indicated times and viremias determined using immunostained TCID₅₀ assays as above. Briefly, mouse serum was titrated in 10-fold serial dilutions into 96-well plates with C6/36 cells and ZIKVs were detected by indirect immunofluorescence as above, except background IgG was blocked prior to addition of the secondary antibody with Goat F(ab) anti-mouse IgG (H&L) (Abcam, Cambridge, United Kingdom).

Antigen-coated ELISA

Anti-ZIKV IgG titers in mouse sera were determined by antigen-coated ELISA. Plates were coated with MR766 antigen in BupH Carbonate-Bicarbonate buffer (Thermo Fisher Scientific, Regensburg, Germany) and incubated O/N at 4°C . After incubation, plates were blocked with 5% skim milk in PBS. Next, the mouse sera were added in triplicates diluted 1:30 in PBS-Tween containing 1% skim milk and incubated for 1 hour at room temperature. After incubation, plates were washed with PBS-Tween. Subsequently, secondary antibody HRP (1:2,000 in PBS-Tween with 1% skim milk) was added and incubated for 1 hour at room

temperature. Samples were washed with PBS-Tween and scored after 1-hour incubation in the dark with ABTS substrate (1:1,000 H₂O₂).

ZIKV_{PRVABC59} challenge

An infectious clone ZIKV_{PRVABC59} (GenBank: MH158237.1) was constructed as described previously [58] and was provided by S. Tajima (Department of Virology I, National Institute of Infectious Diseases, Tokyo, Japan). Infectious virus was recovered by transfection of Vero E6 cells. ZIKV_{PRVABC59} stocks were grown in subconfluent C6/36 mosquito cells maintained in RPMI1640 supplemented with 2% FBS and stored in -80°C. Viral stock titers (TCID₅₀) were determined by 10-fold serial titration in C6/36 cells (2 × 10⁴ cells/well of a 96-well plate) and incubated for 5 days. After incubation, 25 μl from each well was placed into parallel plates containing Vero E6 (2 × 10⁴ cells/well), and the cytopathic effect assessed on day 7.

On day 32 postprimary injections, mice were challenged s.c. base of tail with ZIKV_{PRVABC59} (10³ TCID₅₀ in 100 μl) as described previously [49]. Five mice were mock injected with 100 μl PBS and used as uninfected controls. Mice were weighed at the indicated times. Mouse serum was collected by tail vein bleed and ZIKV_{PRVABC59} titers determined by TCID₅₀ assays as described above. Mice were euthanized on day 80 postprimary infection, testes were removed, photographed, and measured (height × width).

Vaccine safety

To illustrate that the CpG_{max} and UpA_{max} ZIKV mutants do not cause testes damage and are suitable for use as attenuated vaccines, 2 groups of male IFNAR^{-/-} mice (*n* = 6 mice per group) were infected with these ZIKV mutants (10³ TCID₅₀) and testes harvested 49 days post-infection and compared to testes from uninfected mice. qRT-PCR for ZIKV RNA was also performed on the testes as described previously [49].

Statistics

Statistical analyses were done with the software package Prism (v. 9.0.0) and Microsoft Excel 2016 and detailed in the main text and in the relevant figure legend. All two-way analyses of variance (ANOVA) were performed to compare replication of ZIKV variants in multiple cell lines. Outcomes were corrected for multiple comparisons by controlling the false discovery rate (FDR) (*Q* = 0.05). Reported *p*-values for two-way ANOVAs are FDR adjusted *p*-values unless stated otherwise.

Ethics statement for murine experiments

All mouse work was conducted in accordance with the “Australian Code for the care and use of animals for scientific purposes” as defined by the National Health and Medical Research Council of Australia. Mouse experiments and associated statistical treatments were reviewed and approved by the QIMR Berghofer Medical Research Institute animal ethics committee (P2195).

Supporting information

S1 Fig. Antiviral pathways involved in replication of ZIKV mutants. Growth curves on RNaseL knockout (A), OAS1 knockout (B), and OAS3 knockout (C) A549 cells. Cells were infected with mutant ZIKV viruses at 1 RNA/cell. At the indicated dpi, the 50% tissue culture infectious dose was determined by end-point dilution assays. Data points represent the average of 2 biological experiments and the error bars indicate 1 standard error of the mean. (D)

Representative images of ZIKV induced immunoplaques in A549 and A549 ZAP knockout cells. Cells were fixed and stained for ZIKV E protein with primary antibody 4G2 and secondary Alexa Fluor 488 (green). Results of an immunoplaque assay on Vero E6 cells (E). Data points represent the average plaque size, error bars indicate 1 standard error of the mean, and asterisks highlight significant differences from WT ($p < 0.05$, one-way ANOVA with Dunnett post hoc test). Please refer to [S1 Data](#) for the numerical values underlying panels A–C and E. dpi, days postinfection; OAS1, 2'-5'-oligoadenylate synthetase 1; OAS3, 2'-5'-oligoadenylate synthetase 3; RNaseL, ribonuclease L; SCR, scrambled control virus; WT, wild-type; ZIKV, Zika virus.

(TIF)

S2 Fig. Replication of ZIKV with increased CpG dinucleotides has a replication advantage in mosquito cells. *Ae. albopictus* mosquito cell lines: C6/36 (A), U4.4 (B), and RML-12 (C) were infected with the mutant ZIKV viruses at 10 RNA/cell. At the indicated dpi, the 50% tissue culture infectious dose was determined by end-point dilution assays. Data points represent the average of 2 independent biological experiments and the error bars indicate 1 standard error of the mean. Please refer to [S1 Data](#) for the numerical values underlying this figure. dpi, days postinfection; SCR, scrambled control virus; ZIKV, Zika virus.

(TIF)

S3 Fig. Images from DNA gel electrophoresis. Complete and unmodified gel images corresponding to [Fig 4](#). WT ZIKV mixed with either the SCR (A), CpG-high viruses (CpG_1.0 and CpG_max) (B, C), or UpA_max (D). SCR, scrambled control virus; WT, wild-type; ZIKV, Zika virus.

(TIF)

S4 Fig. Replication of ZIKV mutants in *Aedes aegypti*. *Aedes* mosquitoes were offered an infectious blood meal containing equal infectious virus titers of each of the Zika viruses. Mosquito body homogenates (A) and mosquito saliva (B) were inoculated on Vero E6 cells to detect the presence of infectious virus. Bars represent the percentage of ZIKV-positive samples with n varied between 13 and 32 engorged mosquitoes per experimental group. Asterisks represent significant difference from WT (Fisher exact test, $p < 0.01$). The infectious virus titer inside ZIKV-positive mosquito bodies was determined by end-point dilution assay (C). Data points indicate individual mosquito samples and the mean and SEM for each experimental group are displayed. Please refer to [S1 Data](#) for the numerical values underlying this figure.

(TIF)

S1 Table. Composition of mutated regions. CpG and UpA dinucleotide composition of the mutated region in ZIKV and the codon adaptation index compared to both *Homo sapiens* and *Drosophila melanogaster*. Additional numerical values that underlie the values presented in this table are available in [S1 Data](#).

(PDF)

S1 Text. Accession numbers used in this study. Accession numbers that refer to RNA sequences from *Homo sapiens*, *Aedes aegypti*, and the flavivirus genomes that were used to generate [Fig 1A and 1C](#).

(PDF)

S2 Text. Sequence information. Nucleotide sequences of the selected region within Zika virus for all mutant and WT sequences in FASTA format.

(PDF)

S1 Data. Numerical values underlying the results. This spreadsheet contains all numerical values that have made up Fig 1A, 1C, 2A, 2B, 2C, 2D, 2E, 3A, 3B, 3C, 5B, 5C, 5D, 5E, 6B, 6C, 6D, 7A, 7B, 7C, 7D and 7E, panels ABCE in S1 Fig, panels ABC in S2 Fig, panels ABC in S4 Fig, and S1 Table. (XLSX)

Acknowledgments

The authors thank Prof. Andres Merits (University of Tartu) for sharing the ZIKV_{BeH819015} pCCI-SP6 cDNA clone, Prof. Roy Hall and Dr Jody Hobson-Peters (University of Queensland, Australia) for sharing RML-12 *Aedes albopictus* mosquito cells, 4G2 antibody, and MR766 ZIKV antigen, and Dr Astrid Bryon, Dr Mark Sterken, and Marleen Henkens for their support and technical assistance.

Author Contributions

Conceptualization: Jelke J. Fros, Peter Simmonds.

Formal analysis: Jelke J. Fros, Imke Visser, Bing Tang, Kexin Yan, Eri Nakayama, Andreas Suhrbier.

Funding acquisition: Jelke J. Fros, Andreas Suhrbier, Peter Simmonds.

Investigation: Jelke J. Fros, Imke Visser, Bing Tang, Kexin Yan, Eri Nakayama.

Methodology: Jelke J. Fros, Andreas Suhrbier.

Project administration: Monique M. van Oers, Peter Simmonds.

Resources: Tessa M. Visser, Constantianus J. M. Koenraadt, Monique M. van Oers, Gorben P. Pijlman, Andreas Suhrbier.

Supervision: Jelke J. Fros, Constantianus J. M. Koenraadt, Monique M. van Oers, Gorben P. Pijlman, Andreas Suhrbier, Peter Simmonds.

Writing – original draft: Jelke J. Fros.

Writing – review & editing: Imke Visser, Bing Tang, Kexin Yan, Eri Nakayama, Constantianus J. M. Koenraadt, Monique M. van Oers, Gorben P. Pijlman, Andreas Suhrbier, Peter Simmonds.

References

1. Peterson KJ, Lyons JB, Nowak KS, Takacs CM, Wargo MJ, McPeck MA. Estimating metazoan divergence times with a molecular clock. *Proc Natl Acad Sci U S A*. 2004; 101(17):6536–41. Epub 2004/04/16. <https://doi.org/10.1073/pnas.0401670101> PMID: 15084738; PubMed Central PMCID: PMC404080.
2. Goodbourn S, Didcock L, Randall RE. Interferons: cell signalling, immune modulation, antiviral response and virus countermeasures. *J Gen Virol*. 2000; 81(Pt 10):2341–64. <https://doi.org/10.1099/0022-1317-81-10-2341> PMID: 10993923.
3. Blair CD, Olson KE. The role of RNA interference (RNAi) in arbovirus-vector interactions. *Viruses*. 2015; 7(2):820–43. Epub 2015/02/19. <https://doi.org/10.3390/v7020820> PMID: 25690800; PubMed Central PMCID: PMC4353918.
4. Guo Z, Li Y, Ding SW. Small RNA-based antimicrobial immunity. *Nat Rev Immunol*. 2019; 19(1):31–44. Epub 2018/10/12. <https://doi.org/10.1038/s41577-018-0071-x> PMID: 30301972.
5. Sexton NR, Ebel GD. Effects of Arbovirus Multi-Host Life Cycles on Dinucleotide and Codon Usage Patterns. *Viruses*. 2019; 11(7). Epub 2019/07/25. <https://doi.org/10.3390/v11070643> PMID: 31336898; PubMed Central PMCID: PMC6669465.

6. Setoh YX, Amarilla AA, Peng NYG, Griffiths RE, Carrera J, Freney ME, et al. Determinants of Zika virus host tropism uncovered by deep mutational scanning. *Nat Microbiol*. 2019; 4(5):876–87. Epub 2019/03/20. <https://doi.org/10.1038/s41564-019-0399-4> PMID: 30886357; PubMed Central PMCID: PMC6667831.
7. Coulondre C, Miller JH, Farabaugh PJ, Gilbert W. Molecular basis of base substitution hotspots in *Escherichia coli*. *Nature*. 1978; 274(5673):775–80. <https://doi.org/10.1038/274775a0> PMID: 355893.
8. Bird AP. DNA methylation and the frequency of CpG in animal DNA. *Nucleic Acids Res*. 1980; 8(7):1499–504. <https://doi.org/10.1093/nar/8.7.1499> PMID: 6253938; PubMed Central PMCID: PMC324012.
9. Provataris P, Meusemann K, Niehuis O, Grath S, Misof B. Signatures of DNA Methylation across Insects Suggest Reduced DNA Methylation Levels in Holometabola. *Genome Biol Evol*. 2018; 10(4):1185–97. Epub 2018/04/27. <https://doi.org/10.1093/gbe/evy066> PMID: 29697817; PubMed Central PMCID: PMC5915941.
10. Duan J, Antezana MA. Mammalian mutation pressure, synonymous codon choice, and mRNA degradation. *J Mol Evol*. 2003; 57(6):694–701. <https://doi.org/10.1007/s00239-003-2519-1> PMID: 14745538.
11. Beutler E, Gelbart T, Han JH, Koziol JA, Beutler B. Evolution of the genome and the genetic code: selection at the dinucleotide level by methylation and polyribonucleotide cleavage. *Proc Natl Acad Sci U S A*. 1989; 86(1):192–6. <https://doi.org/10.1073/pnas.86.1.192> PMID: 2463621; PubMed Central PMCID: PMC286430.
12. Karlin S, Doerfler W, Cardon LR. Why is CpG suppressed in the genomes of virtually all small eukaryotic viruses but not in those of large eukaryotic viruses? *J Virol*. 1994; 68(5):2889–97. Epub 1994/05/01. <https://doi.org/10.1128/JVI.68.5.2889-2897.1994> PMID: 8151759; PubMed Central PMCID: PMC236777.
13. Simmonds P, Xia W, Baillie JK, McKinnon K. Modelling mutational and selection pressures on dinucleotides in eukaryotic phyla—selection against CpG and UpA in cytoplasmically expressed RNA and in RNA viruses. *BMC Genomics*. 2013; 14:610. Epub 2013/09/12. <https://doi.org/10.1186/1471-2164-14-610> PMID: 24020411; PubMed Central PMCID: PMC3829696.
14. Lobo FP, Mota BE, Pena SD, Azevedo V, Macedo AM, Tauch A, et al. Virus-host coevolution: common patterns of nucleotide motif usage in Flaviviridae and their hosts. *PLoS ONE*. 2009; 4(7):e6282. Epub 2009/07/21. <https://doi.org/10.1371/journal.pone.0006282> PMID: 19617912; PubMed Central PMCID: PMC2707012.
15. Fros JJ, Dietrich I, Alshaikhahmed K, Passchier TC, Evans DJ, Simmonds P. CpG and UpA dinucleotides in both coding and non-coding regions of echovirus 7 inhibit replication initiation post-entry. *Elife*. 2017;6. Epub 2017/09/30. <https://doi.org/10.7554/eLife.29112> PMID: 28960178; PubMed Central PMCID: PMC5659819.
16. Takata MA, Goncalves-Carneiro D, Zang TM, Soll SJ, York A, Blanco-Melo D, et al. CG dinucleotide suppression enables antiviral defence targeting non-self RNA. *Nature*. 2017; 550(7674):124–7. Epub 2017/09/28. <https://doi.org/10.1038/nature24039> PMID: 28953888; PubMed Central PMCID: PMC6592701.
17. Gaunt E, Wise HM, Zhang H, Lee LN, Atkinson NJ, Nicol MQ, et al. Elevation of CpG frequencies in influenza A genome attenuates pathogenicity but enhances host response to infection. *Elife*. 2016;5. <https://doi.org/10.7554/eLife.12735> PMID: 26878752.
18. Witteveldt J, Martin-Gans M, Simmonds P. Enhancement of the replication of HCV replicons of genotypes 1–4 by manipulation of CpG and UpA dinucleotide frequencies and use of cell lines expressing SECL14L2—application for antiviral resistance testing. *Antimicrob Agents Chemother*. 2016. <https://doi.org/10.1128/AAC.02932-15> PMID: 26953209.
19. Atkinson NJ, Witteveldt J, Evans DJ, Simmonds P. The influence of CpG and UpA dinucleotide frequencies on RNA virus replication and characterization of the innate cellular pathways underlying virus attenuation and enhanced replication. *Nucleic Acids Res*. 2014; 42(7):4527–45. Epub 2014/01/29. <https://doi.org/10.1093/nar/gku075> PMID: 24470146; PubMed Central PMCID: PMC3985648.
20. Chiu HP, Chiu H, Yang CF, Lee YL, Chiu FL, Kuo HC, et al. Inhibition of Japanese encephalitis virus infection by the host zinc-finger antiviral protein. *PLoS Pathog*. 2018; 14(7):e1007166. Epub 2018/07/18. <https://doi.org/10.1371/journal.ppat.1007166> PMID: 30016363; PubMed Central PMCID: PMC6049953.
21. Odon V, Fros JJ, Goonawardane N, Dietrich I, Ibrahim A, Alshaikhahmed K, et al. The role of ZAP and OAS3/RNaseL pathways in the attenuation of an RNA virus with elevated frequencies of CpG and UpA dinucleotides. *Nucleic Acids Res*. 2019. Epub 2019/07/06. <https://doi.org/10.1093/nar/gkz581> PMID: 31276592.

22. Luo X, Wang X, Gao Y, Zhu J, Liu S, Gao G, et al. Molecular Mechanism of RNA Recognition by Zinc-Finger Antiviral Protein. *Cell Rep.* 2020; 30(1):46–52 e4. Epub 2020/01/09. <https://doi.org/10.1016/j.celrep.2019.11.116> PMID: 31914396.
23. Zhu Y, Wang X, Goff SP, Gao G. Translational repression precedes and is required for ZAP-mediated mRNA decay. *EMBO J.* 2012; 31(21):4236–46. Epub 2012/10/02. <https://doi.org/10.1038/emboj.2012.271> PMID: 23023399; PubMed Central PMCID: PMC3492732.
24. MacDonald MR, Machlin ES, Albin OR, Levy DE. The zinc finger antiviral protein acts synergistically with an interferon-induced factor for maximal activity against alphaviruses. *J Virol.* 2007; 81(24):13509–18. Epub 2007/10/12. <https://doi.org/10.1128/JVI.00402-07> PMID: 17928353; PubMed Central PMCID: PMC2168828.
25. Li MMH, Aguilar EG, Michailidis E, Pabon J, Park P, Wu X, et al. Characterization of Novel Splice Variants of Zinc Finger Antiviral Protein (ZAP). *J Virol.* 2019; 93(18). Epub 2019/05/24. <https://doi.org/10.1128/JVI.00715-19> PMID: 31118263; PubMed Central PMCID: PMC6714797.
26. Moldovan JB, Moran JV. The Zinc-Finger Antiviral Protein ZAP Inhibits LINE and Alu Retrotransposition. *PLoS Genet.* 2015; 11(5):e1005121. Epub 2015/05/08. <https://doi.org/10.1371/journal.pgen.1005121> PMID: 25951186; PubMed Central PMCID: PMC4423928.
27. Zhu Y, Chen G, Lv F, Wang X, Ji X, Xu Y, et al. Zinc-finger antiviral protein inhibits HIV-1 infection by selectively targeting multiply spliced viral mRNAs for degradation. *Proc Natl Acad Sci U S A.* 2011; 108(38):15834–9. Epub 2011/08/31. <https://doi.org/10.1073/pnas.1101676108> PMID: 21876179; PubMed Central PMCID: PMC3179061.
28. Guo X, Ma J, Sun J, Gao G. The zinc-finger antiviral protein recruits the RNA processing exosome to degrade the target mRNA. *Proc Natl Acad Sci U S A.* 2007; 104(1):151–6. Epub 2006/12/23. <https://doi.org/10.1073/pnas.0607063104> PMID: 17185417; PubMed Central PMCID: PMC1765426.
29. Ficarelli M, Wilson H, Pedro Galao R, Mazzon M, Antzin-Anduetza I, Marsh M, et al. KHNYN is essential for the zinc finger antiviral protein (ZAP) to restrict HIV-1 containing clustered CpG dinucleotides. *Elife.* 2019;8. Epub 2019/07/10. <https://doi.org/10.7554/eLife.46767> PMID: 31284899; PubMed Central PMCID: PMC6615859.
30. Li MM, Lau Z, Cheung P, Aguilar EG, Schneider WM, Bozzacco L, et al. TRIM25 Enhances the Antiviral Action of Zinc-Finger Antiviral Protein (ZAP). *PLoS Pathog.* 2017; 13(1):e1006145. Epub 2017/01/07. <https://doi.org/10.1371/journal.ppat.1006145> PMID: 28060952; PubMed Central PMCID: PMC5245905.
31. Blitvich BJ, Firth AE. Insect-specific flaviviruses: a systematic review of their discovery, host range, mode of transmission, superinfection exclusion potential and genomic organization. *Viruses.* 2015; 7(4):1927–59. Epub 2015/04/14. <https://doi.org/10.3390/v7041927> PMID: 25866904; PubMed Central PMCID: PMC4411683.
32. Colmant AMG, Hobson-Peters J, Bielefeldt-Ohmann H, van den Hurk AF, Hall-Mendelin S, Chow WK, et al. A New Clade of Insect-Specific Flaviviruses from Australian Anopheles Mosquitoes Displays Species-Specific Host Restriction. *mSphere.* 2017; 2(4). Epub 2017/07/18. <https://doi.org/10.1128/mSphere.00262-17> PMID: 28713857; PubMed Central PMCID: PMC5506557.
33. Goertz GP, Abbo SR, Fros JJ, Pijlman GP. Functional RNA during Zika virus infection. *Virus Res.* 2018; 254:41–53. Epub 2017/09/03. <https://doi.org/10.1016/j.virusres.2017.08.015> PMID: 28864425.
34. Harrison JJ, Hobson-Peters J, Colmant AMG, Koh J, Newton ND, Warrilow D, et al. Antigenic Characterization of New Lineage II Insect-Specific Flaviviruses in Australian Mosquitoes and Identification of Host Restriction Factors. *mSphere.* 2020; 5(3). Epub 2020/06/20. <https://doi.org/10.1128/mSphere.00095-20> PMID: 32554715; PubMed Central PMCID: PMC7300350.
35. Khromykh AA, Meka H, Guyatt KJ, Westaway EG. Essential role of cyclization sequences in flavivirus RNA replication. *J Virol.* 2001; 75(14):6719–28. Epub 2001/06/20. <https://doi.org/10.1128/JVI.75.14.6719-6728.2001> PMID: 11413342; PubMed Central PMCID: PMC114398.
36. Trus I, Udenze D, Berube N, Wheler C, Martel MJ, Gerdtts V, et al. CpG-Recoding in Zika Virus Genome Causes Host-Age-Dependent Attenuation of Infection With Protection Against Lethal Heterologous Challenge in Mice. *Front Immunol.* 2019; 10:3077. Epub 2020/02/11. <https://doi.org/10.3389/fimmu.2019.03077> PMID: 32038625; PubMed Central PMCID: PMC6993062.
37. Sim S, Jupatanakul N, Dimopoulos G. Mosquito immunity against arboviruses. *Viruses.* 2014; 6(11):4479–504. Epub 2014/11/22. <https://doi.org/10.3390/v6114479> PMID: 25415198; PubMed Central PMCID: PMC4246235.
38. Cirimotich CM, Scott JC, Phillips AT, Geiss BJ, Olson KE. Suppression of RNA interference increases alphavirus replication and virus-associated mortality in *Aedes aegypti* mosquitoes. *BMC Microbiol.* 2009; 9:49. Epub 2009/03/07. <https://doi.org/10.1186/1471-2180-9-49> PMID: 19265532; PubMed Central PMCID: PMC2660349.

39. Goertz GP, Miesen P, Overheul GJ, van Rij RP, van Oers MM, Pijlman GP. Mosquito Small RNA Responses to West Nile and Insect-Specific Virus Infections in *Aedes* and *Culex* Mosquito Cells. *Viruses*. 2019; 11(3). Epub 2019/03/21. <https://doi.org/10.3390/v11030271> PMID: 30889941; PubMed Central PMCID: PMC6466260.
40. Brackney DE, Scott JC, Sagawa F, Woodward JE, Miller NA, Schilkey FD, et al. C6/36 *Aedes albopictus* cells have a dysfunctional antiviral RNA interference response. *PLoS Negl Trop Dis*. 2010; 4(10): e856. Epub 2010/11/05. <https://doi.org/10.1371/journal.pntd.0000856> PMID: 21049065; PubMed Central PMCID: PMC2964293.
41. Tulloch F, Atkinson NJ, Evans DJ, Ryan MD, Simmonds P. RNA virus attenuation by codon pair deoptimisation is an artefact of increases in CpG/UpA dinucleotide frequencies. *Elife*. 2014; 3:e04531. Epub 2014/12/10. <https://doi.org/10.7554/eLife.04531> PMID: 25490153; PubMed Central PMCID: PMC4383024.
42. Goodier JL, Pereira GC, Cheung LE, Rose RJ, Kazazian HH Jr. The Broad-Spectrum Antiviral Protein ZAP Restricts Human Retrotransposition. *PLoS Genet*. 2015; 11(5):e1005252. Epub 2015/05/23. <https://doi.org/10.1371/journal.pgen.1005252> PMID: 26001115; PubMed Central PMCID: PMC4441479.
43. Goonawardane N, Nguyen D, Simmonds P. Association of zinc-finger antiviral protein (ZAP) binding to viral genomic RNA with attenuation of replication of echovirus 7. *bioRxiv*. 2020:2020.05.14.097329. <https://doi.org/10.1101/2020.05.14.097329>
44. Ruckert C, Ebel GD. How Do Virus-Mosquito Interactions Lead to Viral Emergence? *Trends Parasitol*. 2018; 34(4):310–21. Epub 2018/01/07. <https://doi.org/10.1016/j.pt.2017.12.004> PMID: 29305089; PubMed Central PMCID: PMC5879000.
45. Bick MJ, Carroll JW, Gao G, Goff SP, Rice CM, MacDonald MR. Expression of the zinc-finger antiviral protein inhibits alphavirus replication. *J Virol*. 2003; 77(21):11555–62. Epub 2003/10/15. PubMed Central PMCID: PMC229374. <https://doi.org/10.1128/jvi.77.21.11555-11562.2003> PMID: 14557641
46. Ibrahim A, Fros J, Bertran A, Sechan F, Odon V, Torrance L, et al. A functional investigation of the suppression of CpG and UpA dinucleotide frequencies in plant RNA virus genomes. *Sci Rep*. 2019; 9(1):18359. Epub 2019/12/05. <https://doi.org/10.1038/s41598-019-54853-0> PMID: 31797900; PubMed Central PMCID: PMC6892864.
47. Gonzalez de Pradena A, Sanchez Jimenez A, San Leon D, Simmonds P, Garcia JA, Valli AA. Plant Virus Genome Is Shaped by Specific Dinucleotide Restrictions That Influence Viral Infection. *MBio*. 2020; 11(1). Epub 2020/02/20. <https://doi.org/10.1128/mBio.02818-19> PMID: 32071264; PubMed Central PMCID: PMC7029135.
48. Hogenhout SA, Ammar el D, Whitfield AE, Redinbaugh MG. Insect vector interactions with persistently transmitted viruses. *Annu Rev Phytopathol*. 2008; 46:327–59. Epub 2008/08/06. <https://doi.org/10.1146/annurev.phyto.022508.092135> PMID: 18680428.
49. Hobson-Peters J, Harrison JJ, Watterson D, Hazlewood JE, Vet LJ, Newton ND, et al. A recombinant platform for flavivirus vaccines and diagnostics using chimeras of a new insect-specific virus. *Sci Transl Med*. 2019; 11(522). Epub 2019/12/13. <https://doi.org/10.1126/scitranslmed.aax7888> PMID: 31826984.
50. Simmonds P. SSE: a nucleotide and amino acid sequence analysis platform. *BMC Res Notes*. 2012; 5:50. Epub 2012/01/24. <https://doi.org/10.1186/1756-0500-5-50> PMID: 22264264; PubMed Central PMCID: PMC3292810.
51. Simmonds P, Tuplin A, Evans DJ. Detection of genome-scale ordered RNA structure (GORS) in genomes of positive-stranded RNA viruses: Implications for virus evolution and host persistence. *RNA*. 2004; 10(9):1337–51. Epub 2004/07/27. <https://doi.org/10.1261/ma.7640104> PMID: 15273323; PubMed Central PMCID: PMC1370621.
52. Voronin D, Tran-Van V, Potier P, Mavingui P. Transinfection and growth discrepancy of *Drosophila* Wolbachia strain wMel in cell lines of the mosquito *Aedes albopictus*. *J Appl Microbiol*. 2010; 108(6):2133–41. Epub 2009/12/03. <https://doi.org/10.1111/j.1365-2672.2009.04621.x> PMID: 19951376.
53. Lan Q, Fallon AM. Small heat shock proteins distinguish between two mosquito species and confirm identity of their cell lines. *Am J Trop Med Hyg*. 1990; 43(6):669–76. Epub 1990/12/01. <https://doi.org/10.4269/ajtmh.1990.43.669> PMID: 2267971.
54. Varma MG, Pudney M, Leake CJ, Peralta PH. Isolations in a mosquito (*Aedes pseudoscutellaris*) cell line (Mos. 61) of yellow fever virus strains from original field material. *Intervirology*. 1975; 6(1):50–6. Epub 1975/01/01. <https://doi.org/10.1159/000149453> PMID: 5385.
55. Mutso M, Saul S, Rausalu K, Susova O, Zusinaite E, Mahalingam S, et al. Reverse genetic system, genetically stable reporter viruses and packaged subgenomic replicon based on a Brazilian Zika virus isolate. *J Gen Virol*. 2017; 98(11):2712–24. Epub 2017/10/13. <https://doi.org/10.1099/jgv.0.000938> PMID: 29022864.

56. Goertz GP, van Bree JWM, Hiralal A, Fernhout BM, Steffens C, Boeren S, et al. Subgenomic flavivirus RNA binds the mosquito DEAD/H-box helicase ME31B and determines Zika virus transmission by *Aedes aegypti*. *Proc Natl Acad Sci U S A*. 2019. Epub 2019/09/07. <https://doi.org/10.1073/pnas.1905617116> PMID: 31488709.
57. Gentry MK, Henchal EA, McCown JM, Brandt WE, Dalrymple JM. Identification of distinct antigenic determinants on dengue-2 virus using monoclonal antibodies. *Am J Trop Med Hyg*. 1982; 31(3 Pt 1):548–55. Epub 1982/05/01. <https://doi.org/10.4269/ajtmh.1982.31.548> PMID: 6177259.
58. Kato F, Tajima S, Nakayama E, Kawai Y, Taniguchi S, Shibasaki K, et al. Characterization of large and small-plaque variants in the Zika virus clinical isolate ZIKV/Hu/S36/Chiba/2016. *Sci Rep*. 2017; 7(1):16160. Epub 2017/11/25. <https://doi.org/10.1038/s41598-017-16475-2> PMID: 29170504; PubMed Central PMCID: PMC5701032.
59. Simmonds P, Karakasiliotis I, Bailey D, Chaudhry Y, Evans DJ, Goodfellow IG. Bioinformatic and functional analysis of RNA secondary structure elements among different genera of human and animal caliciviruses. *Nucleic Acids Res*. 2008; 36(8):2530–46. Epub 2008/03/06. <https://doi.org/10.1093/nar/gkn096> PMID: 18319285; PubMed Central PMCID: PMC2377429.